Exploratory Testing of Stress Corrosion Cracking in Stainless Steels at Low Temperature

PUBLICATION NO. FHWA-HRT-24-132

SEPTEMBER 2024

U.S. Department of Transportation
Federal Highway Administration

Research, Development, and Technology
Turner-Fairbank Highway Research Center
6300 Georgetown Pike
McLean, VA 22101-2296

FOREWORD

This report presents the results of a series of exploratory tests carried out to evaluate the possibility of stress corrosion cracking in various grades of stainless steels at close-to-ambient temperatures. This study investigated stress corrosion cracking in stainless steel exposed to salt droplets containing chloride ions at 50 °C (122 °F) and deliquescence relative humidity. The findings indicated that some stainless steel grades can develop stress corrosion cracking and other forms of localized corrosion, whereas others are capable of better withstanding the impact of such a corrosive environment.

Bridge owners, consultants, contractors, and technical experts interested in the use of stainless steel as concrete reinforcement for corrosion resistance will find the information in this report beneficial.

Jean A. Nehme, Ph.D., P.E.
Director, Office of Infrastructure
Research and Development

Recommended citation: Federal Highway Administration, *Exploratory Testing of Stress Corrosion Cracking in Stainless Steels at Low Temperature* (Washington, DC: 2024) https://doi.org/10.21949/1521577

TECHNICAL REPORT DOCUMENTATION PAGE

1. Report No. FHWA-HRT-24-132	2. Government Accession No.	3. Recipient's Catalog No.
4. Title and Subtitle Exploratory Testing of Stress Corrosion Cracking in Stainless Steels at Low Temperature		5. Report Date September 2024 6. Performing Organization Code:
7. Author(s) Rongtang Liu, Arthur Runion, and Frank Jalinoos (ORCID: 0000-0001-8330-7603)		8. Performing Organization Report No.
9. Performing Organization Name and Address SES Group & Associates, LLC 339 Cylamen New Braunfels, TX 78132		10. Work Unit No. 11. Contract or Grant No. DTFH61-17-D-00017
12. Sponsoring Agency Name and Address Office of Infrastructure Research and Development Federal Highway Administration 6300 Georgetown Pike McLean, VA 22101		13. Type of Report and Period Final Report; June 2018–August 2024 14. Sponsoring Agency Code HRDI-10
15. Supplementary Notes The contracting officer's representatives were Chip Becker (formerly HRDI-10) and Frank Jalinoos (HRDI-30; ORCID: 0000-0001-8330-7603).		

16. Abstract

The use of stainless steel as concrete reinforcement has continued to gain momentum in highway construction. The main reason behind stainless steel's popularity is its inherent corrosion resistance. However, stress corrosion cracking (SCC), normally associated with austenitic stainless steel at a high temperature (>100 °C (212 °F)), can occur at a rather low temperature in the presence of concentrated chlorides in commonly used austenitic stainless steels. When stainless steel is used in reinforced concrete, knowledge of the long-term structural integrity of such structures in a corrosive environment is important. The researchers carried out a series of exploratory tests to evaluate the possibility of SCC in various grades of stainless steels at close-to-ambient temperatures. The researchers made U-bend specimens from austenitic stainless steels (grades 304L, 316LN, and XM-28) and austenitic-ferritic duplex stainless steels (grades 2304 and 2205).(1) The specimens were exposed to high-pH salt solutions of calcium chloride, magnesium chloride, and sodium chloride in an evaporative condition. The temperature was elevated to 50 °C (122 °F), simulating the temperature inside a concrete bridge deck in summer. The relative humidity and temperature were close to the deliquescence point of the respective salt. SCC developed in austenitic stainless steels 304L and 316LN, while pitting corrosion perforated XM-28. Austenitic-ferritic duplex stainless steels 2304 and 2205 were resistant to SCC in the studied environment.

17. Key Words Stress corrosion cracking, stainless steel, corrosion, chloride	18. Distribution Statement No restrictions. This document is available to the public through the National Technical Information Service Springfield, VA 22161. https://www.ntis.gov

19. Security Classif. (of this report) Unclassified	20. Security Classif. (of this page) Unclassified	21. No. of Pages 50	22. Price N/A

Form DOT F 1700.7 (8-72) Reproduction of completed page authorized.

SI* (MODERN METRIC) CONVERSION FACTORS

APPROXIMATE CONVERSIONS TO SI UNITS

Symbol	When You Know	Multiply By	To Find	Symbol
		LENGTH		
in	inches	25.4	millimeters	mm
ft	feet	0.305	meters	m
yd	yards	0.914	meters	m
mi	miles	1.61	kilometers	km
		AREA		
in^2	square inches	645.2	square millimeters	mm^2
ft^2	square feet	0.093	square meters	m^2
yd^2	square yard	0.836	square meters	m^2
ac	acres	0.405	hectares	ha
mi^2	square miles	2.59	square kilometers	km^2
		VOLUME		
fl oz	fluid ounces	29.57	milliliters	mL
gal	gallons	3.785	liters	L
ft^3	cubic feet	0.028	cubic meters	m^3
yd^3	cubic yards	0.765	cubic meters	m^3
		NOTE: volumes greater than 1,000 L shall be shown in m^3		
		MASS		
oz	ounces	28.35	grams	g
lb	pounds	0.454	kilograms	kg
T	short tons (2,000 lb)	0.907	megagrams (or "metric ton")	Mg (or "t")
		TEMPERATURE (exact degrees)		
°F	Fahrenheit	5 (F-32)/9 or (F-32)/1.8	Celsius	°C
		ILLUMINATION		
fc	foot-candles	10.76	lux	lx
fl	foot-Lamberts	3.426	$candela/m^2$	cd/m^2
		FORCE and PRESSURE or STRESS		
lbf	poundforce	4.45	newtons	N
lbf/in^2	poundforce per square inch	6.89	kilopascals	kPa

APPROXIMATE CONVERSIONS FROM SI UNITS

Symbol	When You Know	Multiply By	To Find	Symbol
		LENGTH		
mm	millimeters	0.039	inches	in
m	meters	3.28	feet	ft
m	meters	1.09	yards	yd
km	kilometers	0.621	miles	mi
		AREA		
mm^2	square millimeters	0.0016	square inches	in^2
m^2	square meters	10.764	square feet	ft^2
m^2	square meters	1.195	square yards	yd^2
ha	hectares	2.47	acres	ac
km^2	square kilometers	0.386	square miles	mi^2
		VOLUME		
mL	milliliters	0.034	fluid ounces	fl oz
L	liters	0.264	gallons	gal
m^3	cubic meters	35.314	cubic feet	ft^3
m^3	cubic meters	1.307	cubic yards	yd^3
		MASS		
g	grams	0.035	ounces	oz
kg	kilograms	2.202	pounds	lb
Mg (or "t")	megagrams (or "metric ton")	1.103	short tons (2,000 lb)	T
		TEMPERATURE (exact degrees)		
°C	Celsius	1.8C+32	Fahrenheit	°F
		ILLUMINATION		
lx	lux	0.0929	foot-candles	fc
cd/m^2	candela/m2	0.2919	foot-Lamberts	fl
		FORCE and PRESSURE or STRESS		
N	newtons	2.225	poundforce	lbf
kPa	kilopascals	0.145	poundforce per square inch	lbf/in^2

*SI is the symbol for International System of Units. Appropriate rounding should be made to comply with Section 4 of ASTM E380. (Revised March 2003)

TABLE OF CONTENTS

LIST OF FIGURES

LIST OF TABLES

LIST OF ACRONYMS AND ABBREVIATIONS

A	ampere (the unit of electric current)
ACI	American Concrete Institute
$CaCl_2$	calcium chloride
CO_2	carbon dioxide
Cr	chromium
DOT	department of transportation
$FeCl_3$	ferric chloride
FHWA	Federal Highway Administration
ISO	International Organization for Standardization
M	molar
$MgCl_2$	magnesium chloride
mil	1 thousandth of 1 inch
Mo	molybdenum
N	nitrogen
NaCl	sodium chloride
Na_2CO_3	sodium carbonate
$NaHCO_3$	sodium bicarbonate
NaOH	sodium hydroxide
Ni	nickel
PREN	pitting resistance equivalent number
SCC	stress corrosion cracking
UNS	unified numbering system
V	volt (the unit of electric potential)
VTrans	Vermont Agency of Transportation

CHAPTER 1. INTRODUCTION

The service life of many concrete highway structures is limited by their reinforcing steel. Carbon steel has been used as reinforcement in concrete for more than a century. Corrosion of carbon steel reinforcing bars has been a serious issue for many years. The deterioration of the original San Mateo-Hayward bridge in California was studied in 1958.[2] Increased cases of bridge deck deterioration caused by rebar corrosion have been commensurate with accelerated use of deicing salts starting around 1960.[3] The Federal Highway Administration (FHWA), along with many of the State departments of transportation (DOTs), began experimenting with methods to extend the life of concrete carbon steel reinforcing bars in the 1970s as a result of these corrosion issues.[4] With developments of stainless steels in structural applications, the use of stainless steel provides superior durability and reduction in the lifecycle cost of a bridge compared with regular structural steel.

Stainless steel reinforcing bars have been used successfully in corrosive environments for more than 70 yr. Tests by FHWA and various State DOTs show that solid stainless steel reinforcing bars will last at least 100 yr in typical northern State conditions.[4] The obvious advantages of solid stainless steel reinforcing bars are an extremely long life with excellent corrosion resistance, high strength with good ductility, and good concrete bonding.

The use of stainless steel as concrete reinforcement has continued to gain momentum in highway construction.[5,6] Faced with corrosion problems, particularly on bridge decks, some State DOTs have been embracing the application of stainless steel reinforcement. For example, the Vermont Agency of Transportation (VTrans) used solid stainless steel rebars as reinforcement on a concrete deck in 2009.[7] Subsequently, in March 2012 VTrans made stainless steel reinforcing standard for bridge superstructures on high-traffic pavements, replacing epoxy-coated steel.[8] The *2018 VTrans Standard Specifications for Construction* specifies the use of corrosion-resistant reinforcement based on exposure conditions.[9] Recently (2013 and 2016), Virginia DOT used duplex stainless steel 2205 as reinforcement in prestressed bridge piles in the marine environment.[10]

The main reason behind stainless steel's popularity is obviously its inherent corrosion resistance. Stainless steel does not rust because of the interaction between its alloying elements and the environment. Stainless steel contains iron, chromium (Cr), manganese, silicon, carbon, and, in many cases, significant amounts of nickel (Ni) and molybdenum (Mo). These elements react with oxygen from water and air to form a thin, stable film that consists of such corrosion products as metal oxides and hydroxides. Cr plays a dominant role in reacting with oxygen to form this corrosion product film. In fact, all stainless steels contain at least 10-percent Cr.

The presence of the stable film prevents further corrosion by acting as a barrier that limits oxygen and water access to the underlying metal surface. Because the film forms so readily and tightly, even only a few atomic layers reduce the rate of corrosion to low levels. Because the film is much thinner than the wavelength of light, the film is difficult to see, even with the aid of modern instruments, which is the reason why stainless steel's surface looks shiny in visible light. Thus, although the steel is corroded at the atomic level, it appears stainless. Common steel, in contrast, reacts with oxygen to form a relatively unstable iron oxide/hydroxide film that

continues to grow with time and exposure to water and air. As such, this film, otherwise known as rust, grows to sufficient thickness soon after the steel is exposed to water and air, making it easily observable.

The stainless steels for construction are austenitic and austenitic-ferritic stainless steels. The commonly used austenitic stainless steels are 304L (unified numbering system (UNS) S30403), 316LN (UNS S31653), and XM-28 (UNS S24100).[1] 304L is an austenitic stainless steel with a minimum of 18-percent Cr and 8-percent Ni, and the carbon maximum is 0.030 percent. 304L is the most versatile and widely used alloy in the stainless steel family. Ideal for a wide variety of home and commercial applications, 304L exhibits excellent corrosion resistance, ease of fabrication, and outstanding formability. The austenitic stainless steels are also considered to be the most weldable of the high-alloy steels and can be welded by all fusion and resistance welding processes.

316LN (UNS 31653)[1] is a nitrogen (N) alloyed austenitic stainless steel with an addition of Mo. The "L" stands for "low carbon" content. Due to its lower carbon amount, 316L stainless steel has a reduced risk of sensitization (grain boundary carbide precipitation), but at the same time, it loses some of its strength. Stainless steel 316LN is alloyed with N to compensate for the loss of strength.

XM-28 (UNS S24100)[1] is a high-manganese, low-Ni austenitic stainless steel, strengthened by extra N present in the solid solution. Due to lower Ni content compared with the 304- and 316-type stainless steels, XM-28 provides a major cost advantage without adversely affecting corrosion resistance for many applications. High N content provides significantly higher tensile strength and yield strength without adversely affecting elongation and reduction in area (ductility) or nonmagnetic properties. This grade is an excellent choice for rebars used in bridge construction and in the marine environment.

Duplex stainless steels are alloys containing both austenite (face-centered cubic lattice) and ferrite (body-centered cubic lattice) phases in the metallurgical structure with a balanced proportion. The 2205 duplex (UNS S32205) stainless steel contains about 40- to 50-percent ferrite in the annealed condition. The high Cr, Mo, and N contents provide superior corrosion resistance in most environments. The design strength of 2205 is significantly higher than that of 316/316L, thus, often permitting lighter construction.

Alloy 2304 (UNS S32304)[1] is a 23-percent Cr, 4-percent Ni, Mo-free duplex stainless steel. Usually called a lean duplex, 2304 has corrosion resistance properties similar to 316L, but with yield strength nearly double that of austenitic stainless steels. Its duplex microstructure and low-Ni and high-Cr contents also allow duplex 2304 to demonstrate improved stress corrosion-resistant properties compared to stainless steel grades 304 and 316.[1]

Some grades of stainless steel are susceptible to stress corrosion cracking (SCC). SCC occurs in an alloy that is simultaneously under tensile stress and exposed to a corrosive environment, and SCC happens in some specific combination of alloy, environment, and stress conditions.[11,12] Microscopic observation has revealed that SCC is either transgranular or intergranular. SCC, which is normally associated with austenitic stainless steel at high temperatures, can also happen

at a rather low temperature in the presence of concentrated chlorides in commonly used austenitic stainless steels.([13,14])

The cracking develops in the alloys at stresses below their tensile strength. According to ASTM G30, the total strain (ε) on the outside of the bend is approximately calculated as:[15]

$$\varepsilon = T/2R \text{ when } T << R$$

Where:

T = specimen thickness.
R = radius of bend curvature.

In the U-bend specimens used for this study, the total strain on the outside of the bend is approximately 0.125. Per American Concrete Institute (ACI) 318[16] and ASTM A767/A767M,[17] the minimum finished bend diameter for a no. 4 bar is 6*d*, where *d* is the diameter of the rebar. Using the aforementioned formula, the total strain is approximately 1/6, or 0.167, which is higher than the strain in the U-bend specimen. However, the stress in the U-bend specimen and in a bent rebar is circumferential and not uniform. The nonuniformity can be attributed to three factors, according to ASTM G30.[15] First, a stress gradient is present through the specimen thickness, varying from a maximum tension on the outer surface to a maximum compression on the inner surface. Second, the stress varies from zero at the ends of the specimen to a maximum at the center of the bend. Third, the stress may vary across the width of the bend. The stress is even more complicated in a bent rebar due to its ribbed and uneven surface. Determination of actual residual stress in the specimen is beyond the scope of this study.

When a U-bend specimen is stressed, the material in the outer fiber of the bend is strained into the plastic portion of the true-stress–true-strain curve. Some elastic strain relaxation has occurred as a result of allowing the U-bend legs to spring back slightly at the end of the stressing sequence and before the restraining bolts and nuts are installed.

The U-bend specimen contains a large amount of elastic and plastic strain, yet the stress conditions are not usually known, and a wide range of stresses exists in a single specimen. The U-bend specimen is unsuitable for studying the effects of different stresses on SCC. This specimen is most useful for detecting differences between the SCC resistance of different metals in the same environment. Due to the aforementioned reasons, this study does not intend to establish any relation between the behavior of U-bend specimens and rebars in bridge decks.

While stainless steel has a tendency to develop SCC at a relatively high temperature of above 100 °C (212 °F), some austenitic stainless steels suffer SCC at temperatures as low as 30 °C (86 °F).[12] Existing literature[19,19] suggests that duplex stainless steels such as 2304 and 2205 do not develop environmental cracking at temperatures below 70 °C (158 °F). Although rare, duplex stainless steel is also vulnerable to SCC at 50 °C (122 °F). Research on SCC in stainless steel has been mainly focused on environments with high temperatures above 100 °C (212 °F). At low temperatures (≤50 °C (122 °F)), stainless steel may develop localized corrosion in the presence of chloride ions. When stainless steel is used in reinforced concrete, knowing the long-term structural integrity of such structures in a corrosive environment is important.

The main controlling environmental factors for SCC are temperature, humidity, the presence of salt (chloride ions) and its composition, and the time of wetness. Deliquescence is a condition in which a salt absorbs moisture from the air and forms a liquid phase on the salt crystal. As the ambient relative humidity reaches the deliquescence point, the salt particle surface changes gradually with increasing relative humidity until the particle transforms to an aqueous droplet.[20] At the deliquescence condition, salt containing chloride ions can form a concentrated electrolyte layer at the salt-metal interface. The chloride concentration in the electrolyte layer is much higher than the concentration in the bulk solution. For example, at the deliquescence point of magnesium chloride ($MgCl_2$), the concentration of chloride in the electrolyte layer can reach 12 M (1 M is equal to 1 mol/L) at ambient temperature.[18] Such a high concentration of chloride is not found in bulk solution at the same temperature.

This study assessed the environmental condition and the application limits of commonly used stainless steels for concrete reinforcement. The stainless steel grades tested were austenitic stainless steels 304L, 316LN, and XM-28, and austenitic-ferritic (duplex) stainless steels 2205 and 2304.[1] The researchers carried out a series of exploratory testing t to evaluate the possibility of SCC in stainless steels at close-to-ambient temperature. U-bend specimens were constantly exposed to salts such as calcium chloride ($CaCl_2$), $MgCl_2$, and sodium chloride (NaCl) in an evaporative condition. The temperature was elevated to 50 °C (122 °F), simulating the temperature inside a concrete bridge deck in the summer. The U-bend test serves as a prelude to the cracked beam test described in ASTM A955 A3.[21]

CHAPTER 2. EXPERIMENTAL SETUP

U-bend specimens (based on ASTM G30-97[15]) were made from stainless steels 2304, 2205, XM-28, 316LN, and 304L.[1] The specimens were exposed to an evaporative condition. The temperature was elevated to 50 °C (122 °F), simulating the temperature inside a concrete bridge deck in the summer. The stainless steel grades and their chemical composition are listed in table 1.

Table 1. Stainless steel stocks.

Stainless Steel Grade		Microstructure	Alloying Chemical Composition (weight percent)			
ASTM	UNS		Cr	Mo	Ni	N
304L	S30403	Austenite	18.2	0.3	8.0	0.08
316LN	S31653	Austenite	17.7	2.1	10.2	0.12
XM-28	S24100	Austenite	18.1	0.0	1.0	0.29
2304	S32304	Duplex	22.8	0.3	3.6	0.17
2205	S32205	Duplex	21.6	2.6	4.7	0.18

U-BEND SPECIMEN FABRICATION

The specimen fabrication process is described in ASTM G30-97.[15] The stock material used for fabricating the specimens was reinforcing bars. The researchers cut a rectangular strip from the bar-shaped stock longitudinally along the direction of rolling using wire electrical discharge machining. The strip was cut into plates with the following dimensions: 1.6 mm (1/16 inch) thick, 19.0 mm (3/4 inch) wide, and 63.5 mm (2-1/2 inch) long (before bending) with two 9.5-mm (3/8-inch)-diameter holes located 12.7 mm (1/2 inch) from each end and centered. Each plate was stamped with the steel grade number for identification. The plate was bent 180 degrees around a 6.35-mm (1/4-inch) radius and then kept in the constrained U-shape with stainless steel fasteners and insulating bushings (figure 1).

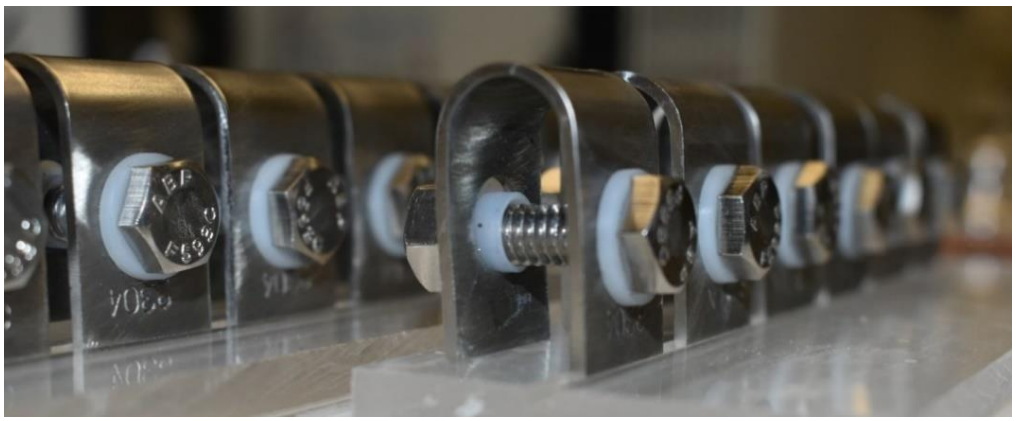

Source: FHWA.

Figure 1. Photo. U-bend specimens.

The surface of the steel was polished with 400-grit sandpaper to eliminate machine marks. The assembled U-bend specimen was degreased before being subjected to the corrosive environment. Acetone, which is chemically inert to steel, was used for degreasing. Each specimen was examined under an optical microscope for any mechanical cracking.

TEMPERATURE AND RELATIVE HUMIDITY OF THE ENVIRONMENT

The relative humidity and temperature were controlled to maintain deliquescent points of each salt that was deposited on the steel surface of the U-bend specimens. From existing literature, the deliquescent point of a few common salts (e.g., NaCl) at room temperature was determined.[12] At elevated temperature, the relative humidity was controlled so that the salt was unable to absorb too much moisture from the environment. The goal was to create an environment so that the salt deposit maintained a saturated liquid on the steel surface.

The drop evaporation test creates an atmospheric exposure condition that is defined by the temperature, relative humidity, and deposit composition. ($CaCl_2$, $MgCl_2$, and NaCl were used as chloride deposits.) This test method is described in International Organization for Standardization (ISO) 15324-2000, *Corrosion of Metals and Alloys—Evaluation of Stress Corrosion Cracking by the Drop Evaporation Test*.[22]

In aqueous solution, the solubility of $CaCl_2$ is 745 g/L (6 lb/gal) at 20 °C (68 °F), 811 g/mL (7 lb/gal) at 25 °C (77 °F), and 1,345 g/L (11 lb/gal) at 60 °C (140 °F), and the mass percentage of chloride in $CaCl_2$ is 64 percent. The solubility of $MgCl_2$ is 543 g/L (5 lb/gal) at 20 °C (68 °F) and 726 g/L (6 lb/gal) at 100 °C (212 °F), and the mass percentage of chloride in $MgCl_2$ is 74.5 percent. The solubility of NaCl in water is 360 g/L (3 lb/gal) at 25 °C (77 °F). The mass percentage of chloride in NaCl is 60.7 percent.

The solutions used for depositing chloride on the steel surface are listed in table 2. The chloride concentration in the $MgCl_2$ and $CaCl_2$ solutions was 12 M (45 mol/gal) and in the NaCl solution was 6.2 M (23 mol/gal). The higher concentration cannot be achieved in NaCl because it reaches saturation.

Table 2. Chloride concentration in solutions.

Salt	Salt in 1-L Solution (g (lb))	Chloride Concentration (M (mol/gal))	Chloride Concentration in Solution (g/L (lb/gal))
$CaCl_2$	665.9 (1.5)	12 (45)	426.0 (3.6)
$MgCl_2$	571.2 (1.3)	12 (45)	426.0 (3.6)
NaCl	360.0 (0.8)	6.2 (23)	218.8 (1.8)

Sodium hydroxide (NaOH) solution was used to achieve high pH in the salt solutions. Measured amounts of salt were added to the pH 13 NaOH solution. The solutions were kept in airtight containers to prevent carbonation, since high-alkali aqueous solution (pH > 10) reacts directly with carbon dioxide (CO_2) in the air to form sodium bicarbonate ($NaHCO_3$), which further reacts with the alkali to form sodium carbonate (Na_2CO_3) by neutralization. The chemical reaction can be presented as:

$$NaOH+CO_2=NaHCO_3$$

$$NaHCO_3+NaOH=Na_2CO_3+H_2O$$

Therefore, the pH of the NaOH solution decreases with time if the solution is exposed to air. In the laboratory, the research team monitored the pH change by periodically measuring the pH of the NaOH solutions of 10 mL in open beakers. The pH of the solutions decreased from pH 13 to pH 9 in 28 h, and to pH 8.5 in 144 h, and was stable at this value for the remaining 10 d of monitoring.

Droplets of pH 13 salt solutions were placed on clean glass plates in a sealed glass container. After 8 w of exposure to the air in the container, the solutions were neutralized to various degrees of much lower pH, as shown in table 3. Although the pH of the salt solution droplets placed on the U-bend was not directly measured, the researchers expected that neutralization occurred, and the pH lowered to the same level as that in the mockup droplets.

Table 3. pH of salt solutions.

Solution	Initial	7 d	14 d	28 d	42 d
$CaCl_2$+NaOH	13	12	10	9.5	8.5
$MgCl_2$+NaOH	13	12	9.5	9	7.0
NaCl+NaOH	13	12.5	12.0	10	11.5

Two 30-µL (0.001-fl oz) droplets of salt solution were placed on the arch of the U-bend, as shown in figure 2. The volume of the droplets was measured with a precision syringe to control the volume. The wetted area by the droplet on the U-bend was about 20 mm^2 (0.031 in^2), but some droplets shrunk to about 12.5 mm^2 (0.019 in^2) due to evaporation.

Source: FHWA.

Figure 2. Photo. U-bend specimen with two saltwater droplets.

The U-bends were stored in a desiccator, as shown in figure 3. Inside the desiccator, a beaker containing the same salt solution was placed next to the specimens. A digital meter was placed in the desiccator to record the temperature and humidity. The elevated temperature was achieved in an insulated hotbox with a halogen lamp providing heating, as shown in figure 4. A programmable controller turned the lamp on and off so that the temperature in the hotbox stayed constant once stabilized. A small fan was placed in the middle of the upper rack in the hotbox so that air circulated to keep the temperature evenly distributed inside the box.

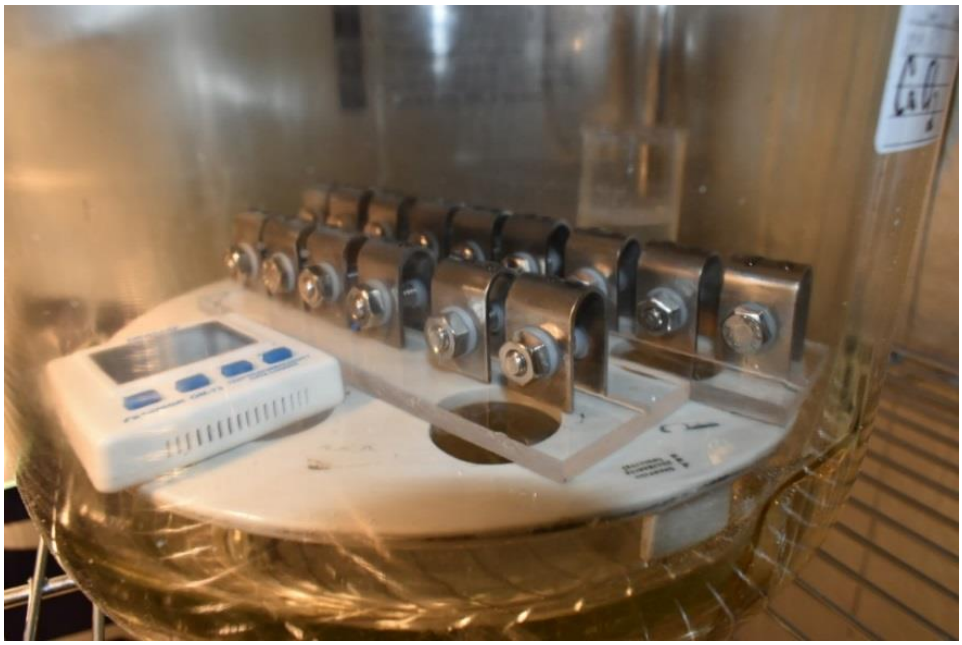

Source: FHWA.

Figure 3. Photo. U-bend specimens in a desiccator.

Source: FHWA.

Figure 4. Photo. Desiccator in a temperature-control hotbox.

The temperature and relative humidity in the sealed desiccators were monitored. Periodically the desiccators were opened to retrieve the digital monitor to download the data, and in the case of NaCl droplets, to remount the droplets as some had rolled off the U-bend specimens. The temperature reached stability in 2 h, but the relative humidity needed 12 h to stabilize. The temperature and relative humidity at the stable state are shown in table 4.

Table 4. Temperature and relative humidity at stable state.

Solution	Temperature (°C (°F))	Relative Humidity (percent)
$CaCl_2$+NaOH	50±1 (122±0.5)	30±2
$MgCl_2$+NaOH	50±1 (122±0.5)	35±2
NaCl+NaOH	50±1 (122±0.5)	75±2

CHAPTER 3. RESULTS AND ANALYSES

DEVELOPMENT OF SCC

A stereo microscope with sufficient magnification and image capturing capability was used to observe the cracks in the stainless steel U-bend specimens and document the corrosion damage and SCC development.

Metallographic analysis was carried out once the samples were polished, allowing a clear image under the microscope for determining SCC in the stainless steels. Various etchants were applied to the polished surface to determine the type of cracking that occurred in relation to the steel grain boundaries.

Periodic observation was carried out following the initial droplet placement, and additional solution was added if the droplet rolled off the surface or evaporated to a much smaller amount. In most cases with $CaCl_2$ and $MgCl_2$ solutions, the droplet became gel-like and remained firmly on the U-bend arch (as shown in figure 5 and figure 6). However, NaCl solution did not form a gel-like droplet, and often the liquid solution would either roll off the surface or evaporate, and salt crystals became visible (as shown in figure 7). The NaCl solution was frequently replenished for some of the U-bend specimens.

Corrosion occurred close to the center of the droplet, as shown in figure 5 and figure 6. The anode was located close to the center of the droplet because the supply of oxygen was limited by the liquid phase of the droplet. The rim of the droplet, being close to air, became the cathode because oxygen was readily available. The brown-colored iron corrosion products spread between the anodic and cathodic regions. The anodic area was not always perfectly centered in the area covered by the droplet. Stainless steels are passive by nature, and pitting corrosion initiates at anodic sites.

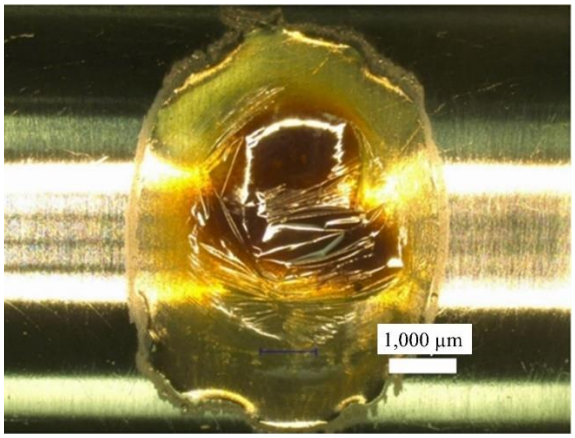

Source: FHWA.
1,000 µm = 39 mils (1 thousandth of 1 inch).

Figure 5. Photomicrograph. High-pH $CaCl_2$ droplet on a 304L stainless steel U-bend specimen.

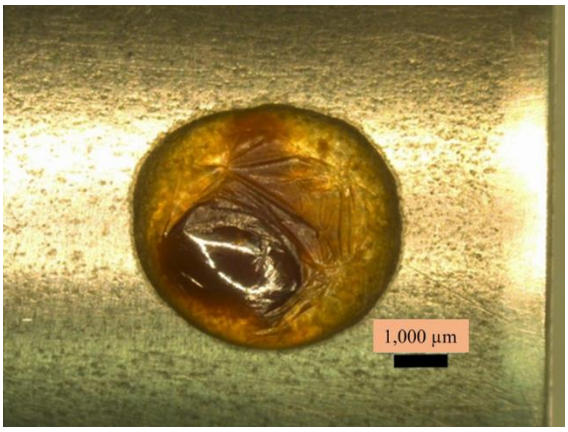

Source: FHWA.
1,000 µm = 39 mils.

Figure 6. Photomicrograph. $CaCl_2$ solution formed gel-like droplet on 316LN stainless steel U-bend specimen.

The NaCl droplets on the U-bends sometimes evaporated, and salt crystals form, as shown in figure 7.

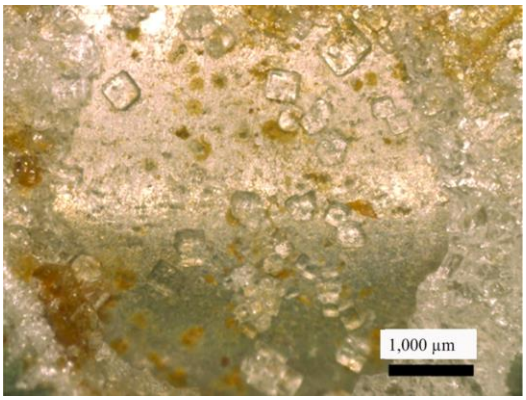

Source: FHWA.
1,000 µm = 39 mils.

Figure 7. Photomicrograph. NaCl droplet evaporated, and salt crystals formed, on a 316LN stainless steel U-bend specimen.

Oxygen is available in the air surrounding the droplet. The dissolved oxygen is concentrated near the edge of the droplet. Diffusion of oxygen into the interior of the droplet is limited. In a perfectly circular droplet, the anode is at the center and the cathode is at the peripheral area of the droplet. However, the droplet on the U-bend was rarely a perfect circle, and the outer surface of the droplet was not spherical. Therefore, the most oxygen-depleted site was usually off-center, resulting in the initiating anodic site being offset from the geometric center of the droplet. The stress in the U-bend assisted the corrosion reaction, increasing the chances that an anodic reaction would take place at the center of the droplet-covered area.

Periodically, the U-bends were removed from the desiccators and examined microscopically. Figure 8 shows some visible cracks extending beyond the boundary of the salt droplet. Localized corrosion, commonly in the form of pitting, was also observed on some of the stainless steel specimens (figure 9).

On some U-bends, pitting corrosion was observed to initiate near the edge of the droplet, as shown in figure 9. This circumstance occurred when the droplet relocated due to rolling on the U-bend, a rough spot on the U-bend for the saltwater to stay, or evaporation.

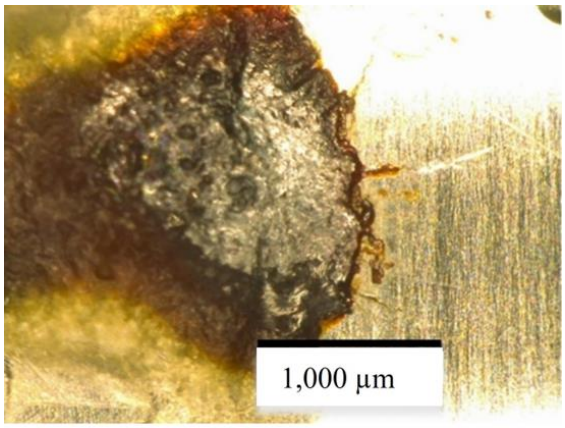

Source: FHWA.
1,000 µm = 39 mils.

Figure 8. Photomicrograph. Cracks developed on a 304L stainless steel specimen exposed to high-pH $MgCl_2$ droplet.

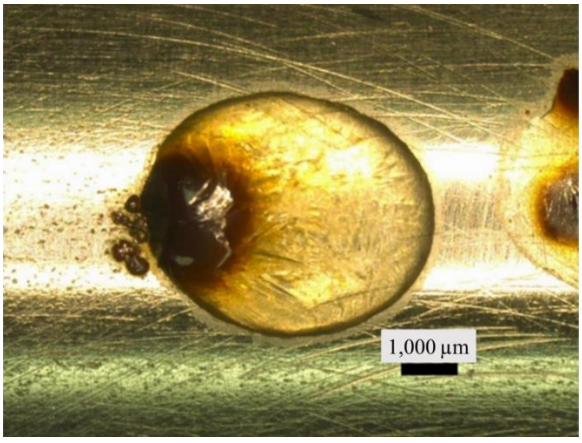

Source: FHWA.
1,000 µm = 39 mils.

Figure 9. Photomicrograph. Pitting and rust formed at the edge of a high-pH $CaCl_2$ droplet on 316LN stainless steel.

Exposure to $CaCl_2$, $MgCl_2$, and NaCl at 50 °C (122 °F)

Two batches of U-bend specimens were tested. On the first batch of specimens, salt droplets with a pH of 7 were mounted on the U-bends. The specimens were examined periodically under a microscope to observe corrosion damages. Testing on the first batch of specimens ended after 25 w of exposure when cracks severed some U-bends.

The high-pH salt solutions were mounted on the second batch of specimens. After 1 yr of exposure, the U-bend specimens were removed from the desiccators, and the salt solution deposits were wiped clean. As shown in figure 10, the stainless steels showed varying degrees of corrosion. The findings in the following subsections pertain to specimens exposed to high-pH salt solutions. The SCC pattern and other forms of corrosion were essentially the same for both pH cases, although the time of corrosion initiation and degree of corrosion damage were slightly different. Therefore, primary attention was paid to the corrosion under the high-pH salt solutions, unless specified otherwise.

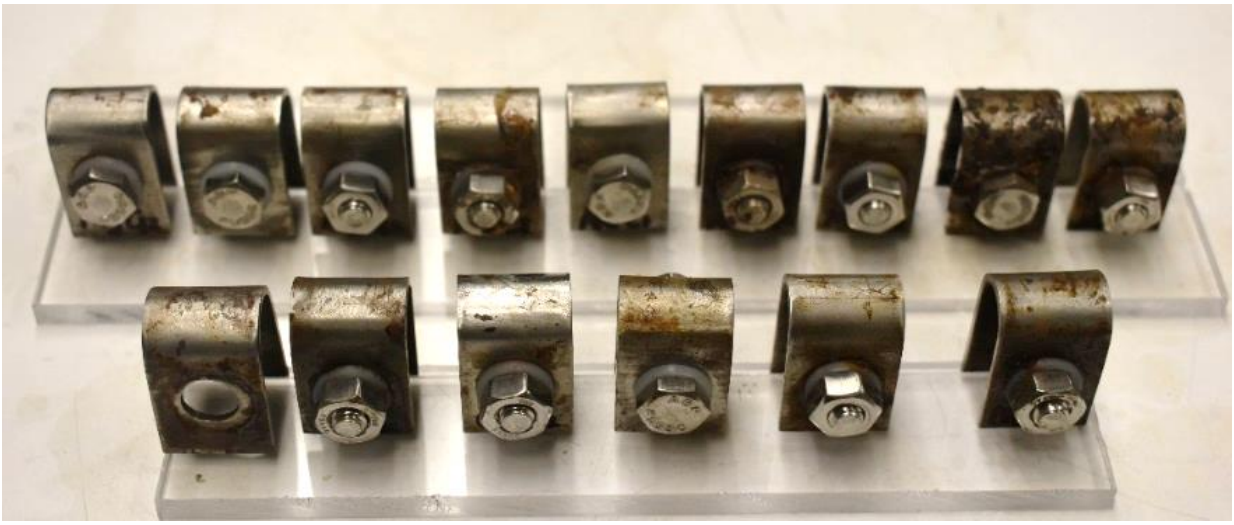

Source: FHWA.

Figure 10. Photo. U-bends after 1 yr of exposure.

304L and 316LN

Stress corrosion cracks were found on the specimens of stainless steel grades[(1)] 304L and 316LN exposed to $CaCl_2$ and $MgCl_2$ when the initial microscopic examination was carried out after 8 w of exposure. The cracks were located at the center area of the U-bend (crown or apex of the arch) where the stress was maximized. Cracks initiated from a pit, as shown in figure 11 and figure 12. The crack branched out as it propagated along the crown of the arch. Although no cracks were observed on NaCl-contaminated stainless steels, many pits were developed on the crown of the U-bend, as shown in figure 13.

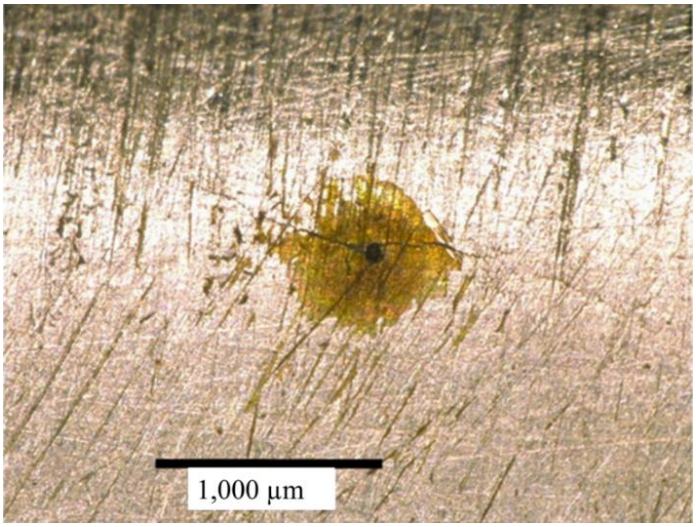

Source: FHWA.
1,000 µm = 39 mils.

Figure 11. Photomicrograph. Cracks initiated from a pit in stainless steel 304L exposed to $MgCl_2$ droplet.

Source: FHWA.
1,000 µm = 39 mils.

Figure 12. Photomicrograph. Pits and cracks developed in stainless steel 316LN exposed to $MgCl_2$ droplet.

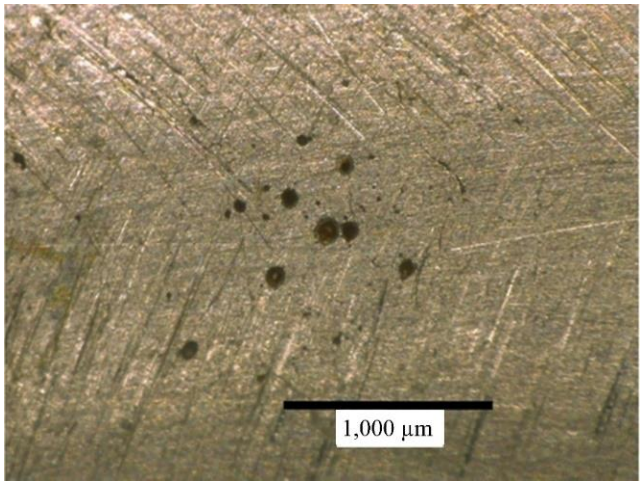

Source: FHWA.
1,000 µm = 39 mils.

Figure 13. Photomicrograph. Pitting on 304L stainless steel exposed to NaCl droplet.

SCC caused severe damage to the austenitic stainless steels[(1)] 304L and 316LN by $CaCl_2$ and $MgCl_2$. Cracking was more extensive in the 304L stainless steel specimens than in the 316LN ones, as demonstrated in figure 14 and figure 15. Both U-bends were exposed to $MgCl_2$ for the same period, but the cracks were wider on the 304L specimen. The same pattern was not observed on U-bends exposed to $CaCl_2$, as shown in figure 16 and figure 17.

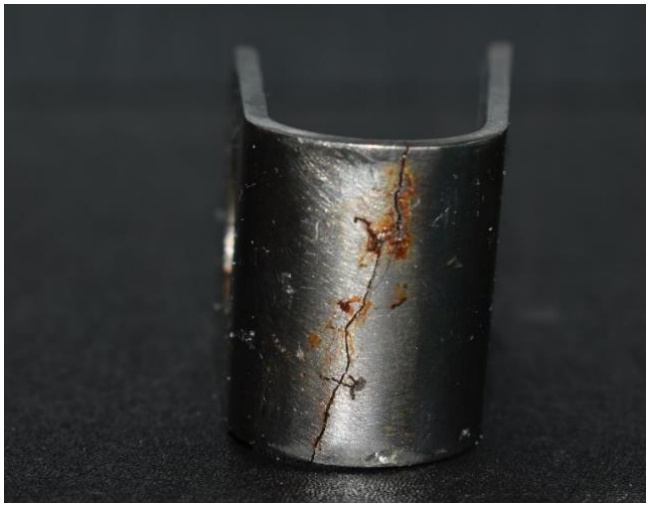

Source: FHWA.

Figure 14. Photo. Cracking through U-bend specimen with high-pH $MgCl_2$ droplet on 304L stainless steel.

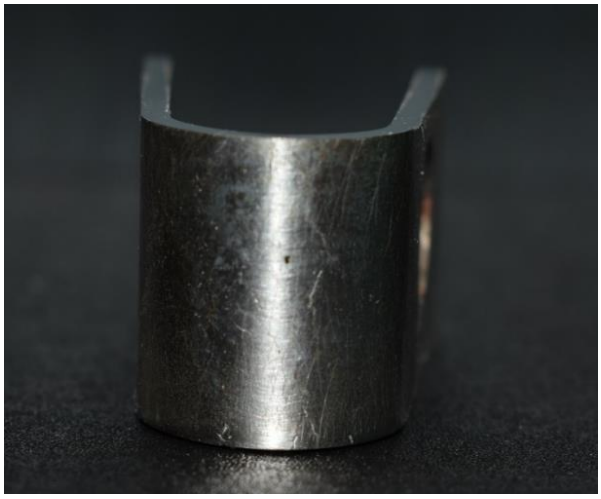

Source: FHWA.

Figure 15. Photo. Cracking through U-bend specimen with high-pH $MgCl_2$ droplet on 316LN stainless steel.

Source: FHWA.

Figure 16. Photo. Cracking through U-bend specimen with high-pH $CaCl_2$ droplet on 304L stainless steel.

Source: FHWA.

Figure 17. Photo. Cracking through U-bend specimen with high-pH $CaCl_2$ droplet on 316LN stainless steel.

Metallographic examination revealed extensive cracking caused by stress corrosion. Cracks in stainless steel 304L[(1)] samples exposed to $CaCl_2$ were wider than those exposed to $MgCl_2$, as compared between figure 18 and figure 19. Although both U-bends fractured after 1 yr of exposure, $MgCl_2$ created much more extensive cracking. Intergranular and intragranular cracks are observed in these specimens, as shown in figure 20 and figure 21.

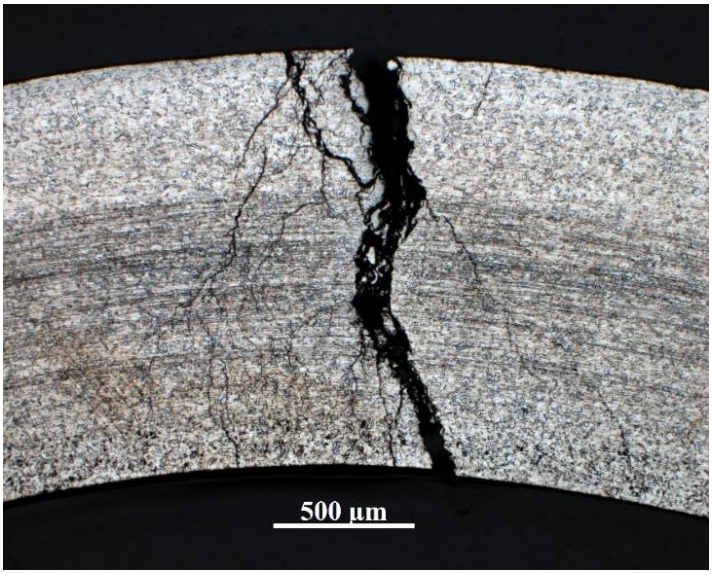

Source: FHWA.
500 µm = 20 mils.

Figure 18. Photomicrograph. Cracks in U-bend specimen with high-pH $CaCl_2$ droplet on 304L stainless steel.

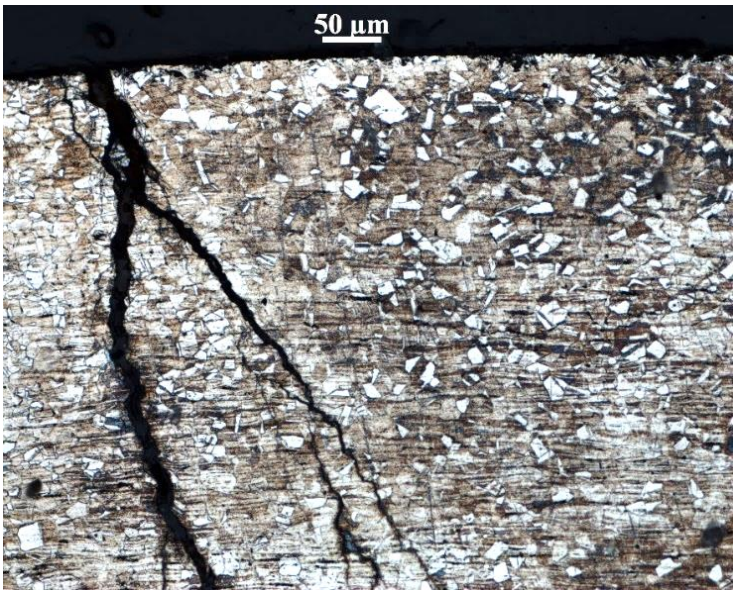

Source: FHWA.
50 µm = 2 mils.

Figure 19. Photomicrograph. Cracks in U-bend specimen with high-pH $MgCl_2$ droplet on 304L stainless steel.

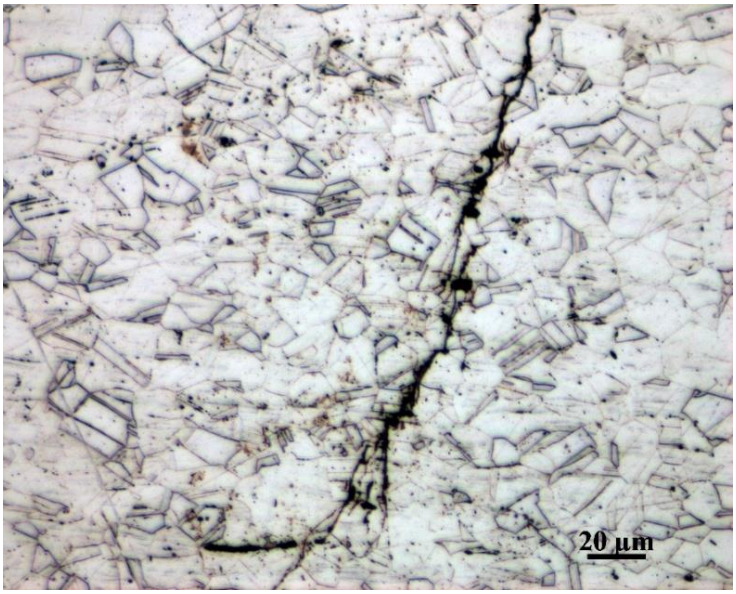

Source: FHWA.
20 µm = 0.8 mil.

Figure 20. Photomicrograph. Intergranular and intragranular cracks through U-bend specimen with high-pH $CaCl_2$ droplet on 304L stainless steel.

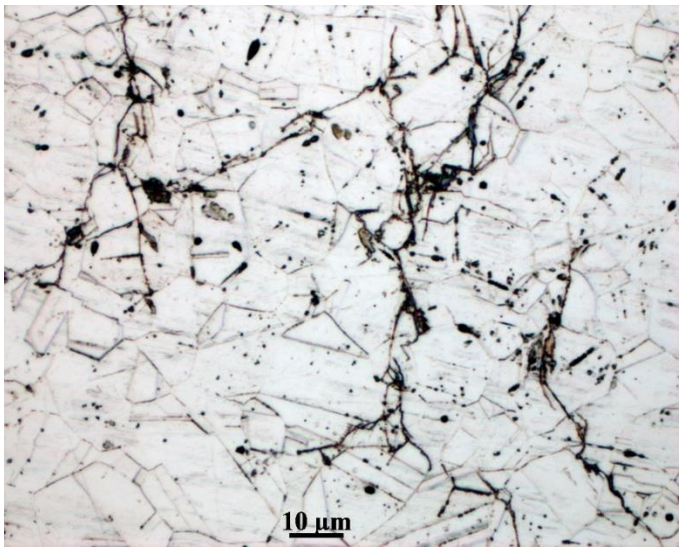

Source: FHWA.
10 µm = 0.4 mil.

Figure 21. Photomicrograph. Intergranular and intragranular cracks through U-bend specimen with high-pH $CaCl_2$ droplet on 304L stainless steel.

The stainless steel 316LN[(1)] specimens exposed to $CaCl_2$ developed multiple major cracks under the salt droplet, as shown in figure 22. The cracks then branched out as they propagated deep into the bulk of the steel. The cracks in the stainless steel 316LN specimens exposed to $MgCl_2$ were more numerous than those exposed to $CaCl_2$, as shown in figure 23. Many cracks penetrated the whole depth of the U-bend specimen.

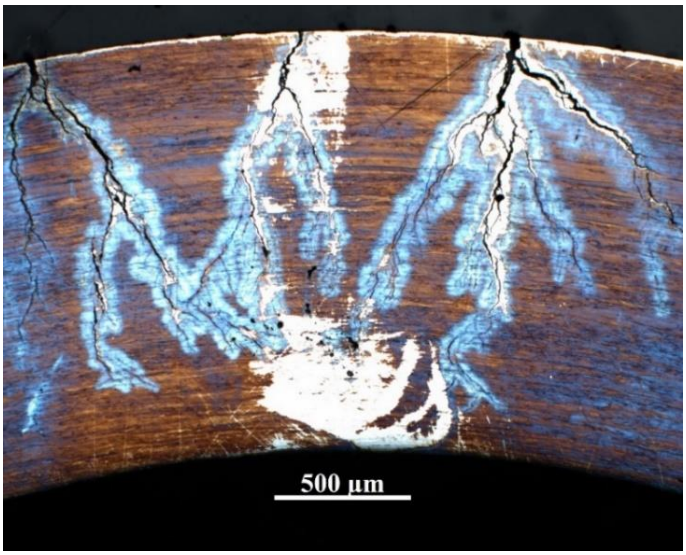

Source: FHWA.
500 µm = 20 mils.

Figure 22. Photomicrograph. Multiple major cracks through U-bend specimen with high-pH $CaCl_2$ droplet on 316LN stainless steel.

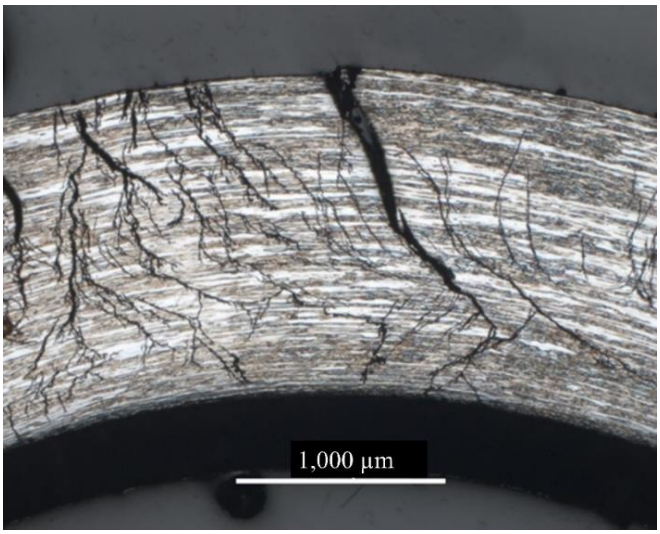

Source: FHWA.
1,000 µm = 39 mils.

Figure 23. Photomicrograph. Cracking in stainless steel 316LN exposed to $MgCl_2$ droplet.

XM-28

Although stress corrosion cracks were not found on the XM-28 stainless steel,[(1)] severe pitting corrosion did develop, as shown in figure 24. Pitting corrosion was not limited to the crown of the arch, but also occurred elsewhere, including the legs of the U-bend where stress was low. Metallographic examination did not find any sign of cracks, but deep pits were formed in the stainless steel structure as shown in figure 25, figure 26, and figure 27. After 1 yr of exposure, pitting corrosion perforated the stainless steel, as shown in figure 28 and figure 29.

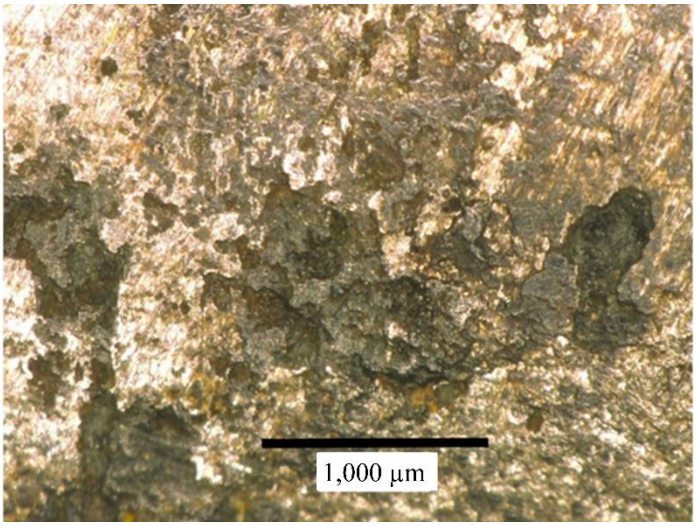

Source: FHWA.
1,000 µm = 39 mils.

Figure 24. Photomicrograph. Pitting corrosion of stainless steel XM-28 exposed to NaCl solution.

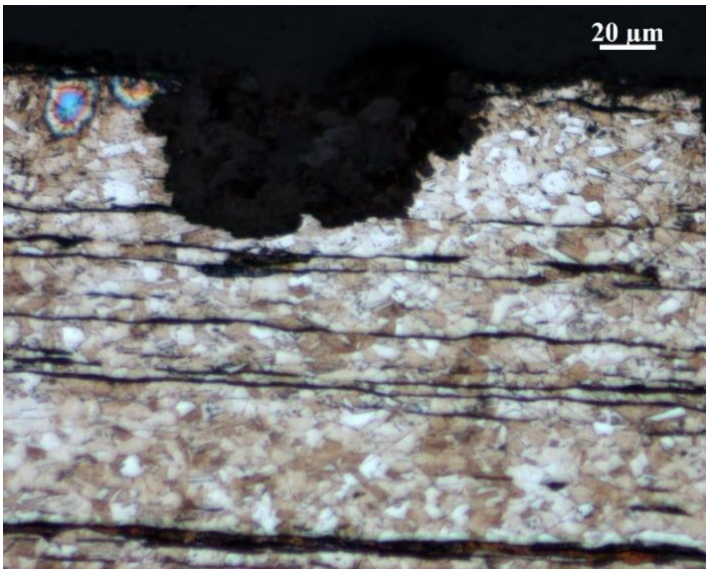

Source: FHWA.
20 µm = 0.8 mil.

Figure 25. Photomicrograph. Pitting corrosion of stainless steel XM-28 exposed to 60-µm (2.4-mil) $MgCl_2$ droplet.

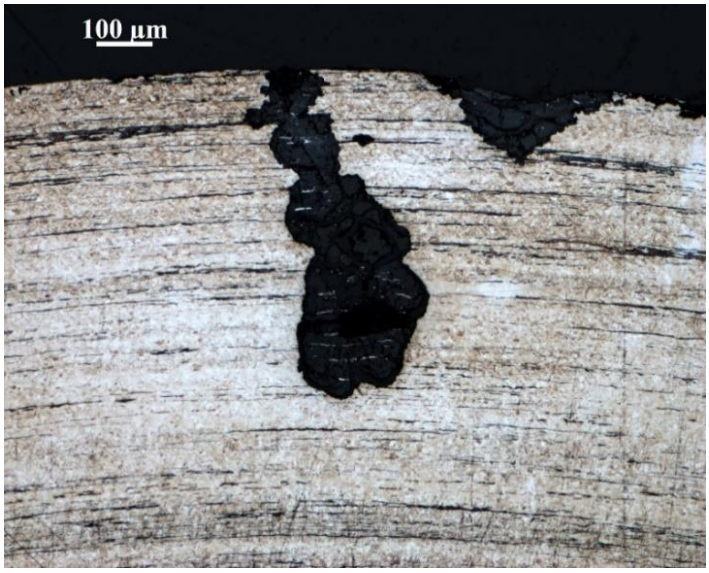

Source: FHWA.
100 µm = 4 mils.

Figure 26. Photomicrograph. Pits in stainless steel XM-28 exposed to 580-µm (23-mil) NaCl droplet.

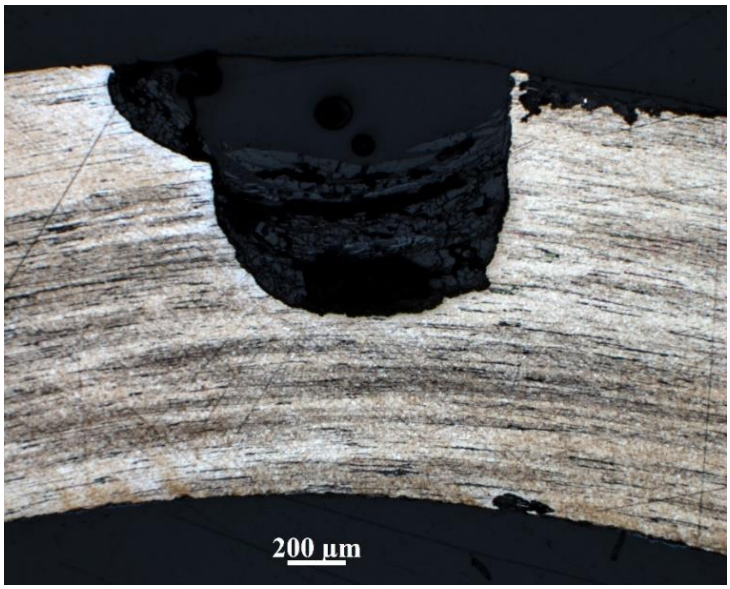

Source: FHWA.
200 µm = 8 mils.

Figure 27. Photomicrograph. Pits in stainless steel XM-28 exposed to 900-µm (35-mil) NaCl droplet.

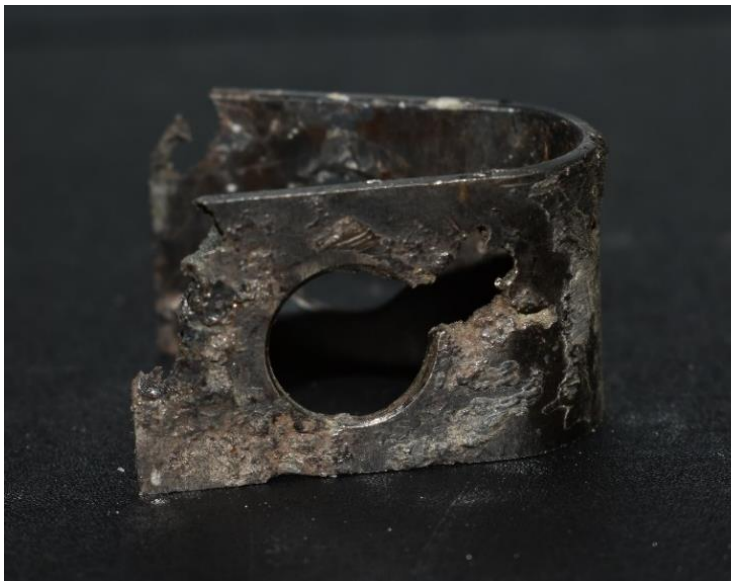

Source: FHWA.

Figure 28. Photo. Localized corrosion on U-bend specimen with high-pH $MgCl_2$ droplet on XM-28 stainless steel.

Source: FHWA.

Figure 29. Photo. Localized corrosion on U-bend specimen with high-pH NaCl droplet on XM-28 stainless steel.

Duplex stainless steel grades 2205 and 2304[(1)] showed no sign of SCC. The stainless steel 2304 specimens developed pitting corrosion, as seen in figure 30 and figure 31, although the pits were usually shallow with depth less than 10 μm (0.4 mil), as shown in figure 32.

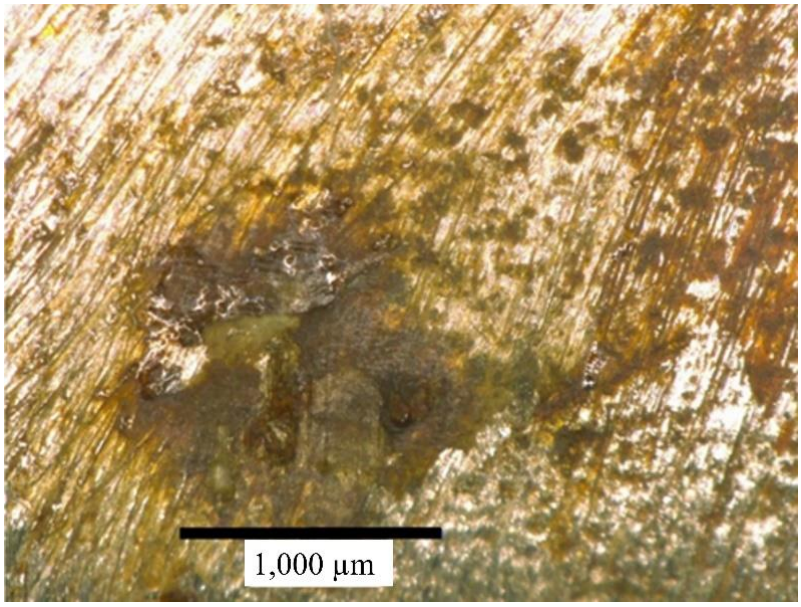

Source: FHWA.
1,000 μm = 39 mils.

Figure 30. Photomicrograph. Pitting corrosion on stainless steel 2205 exposed to $MgCl_2$ droplet.

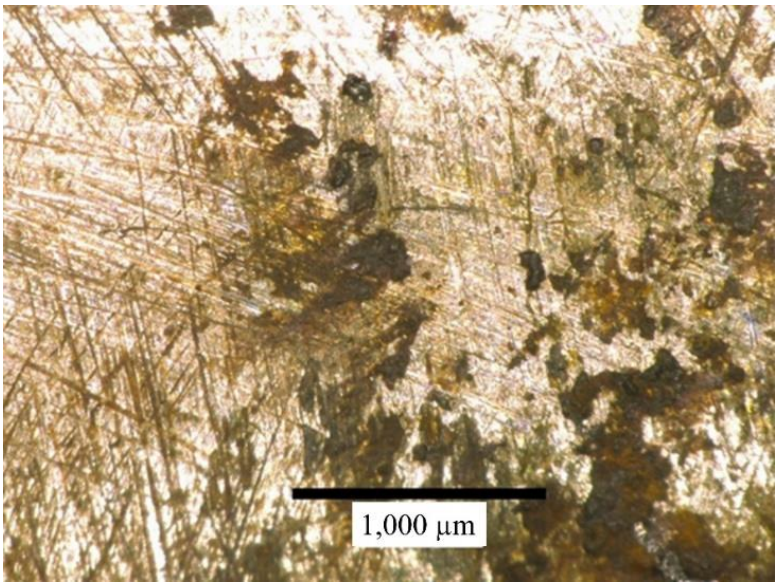

Source: FHWA.
1,000 µm = 39 mils.

Figure 31. Photomicrograph. Pitting corrosion on stainless steel 2304 exposed to NaCl droplet.

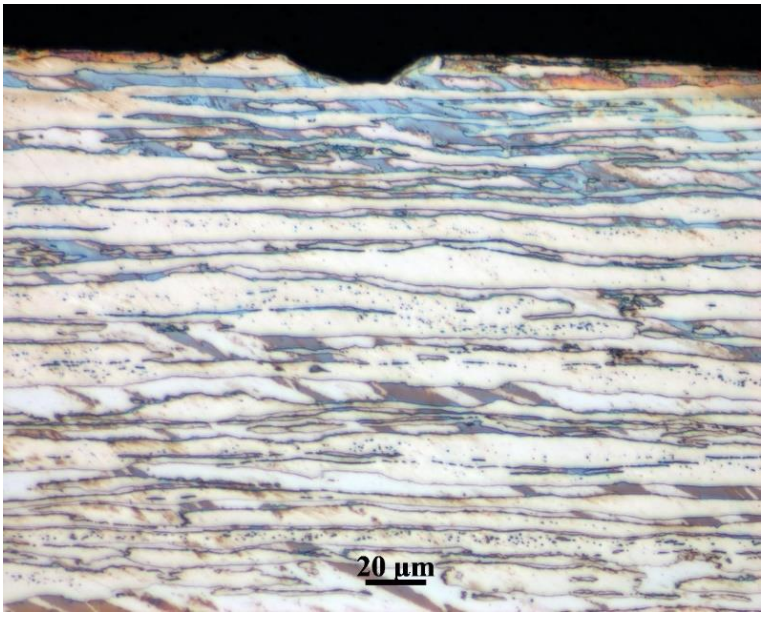

Source: FHWA.
20 µm = 0.8 mil.

Figure 32. Photomicrograph. Stainless steel 2304 exposed to $MgCl_2$ droplet.

In addition to sporadic shallow pits, on rare occasions, corrosion hollowed out part of the steel from beneath the surface, as shown in figure 33. The stainless steel was electrolytically etched with 40-percent aqueous NaOH solution, showing blue austenite and yellow ferrite.

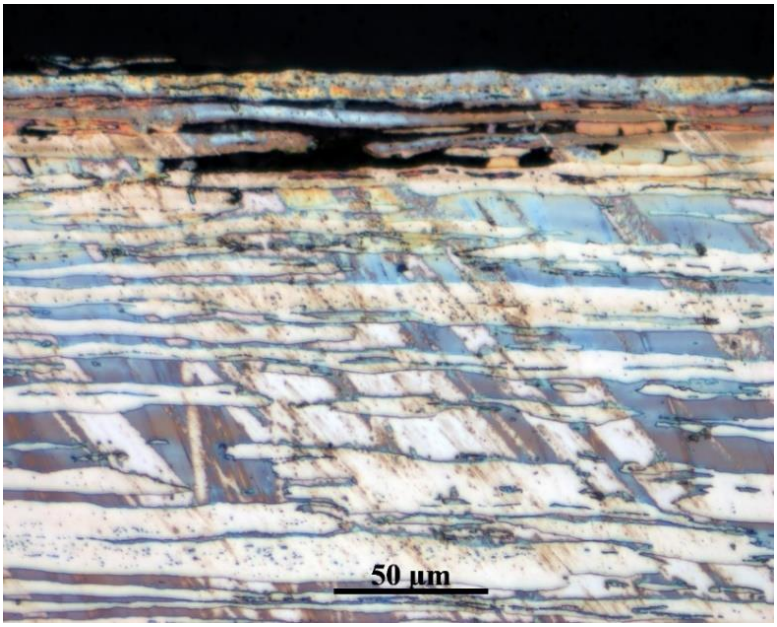

Source: FHWA.
50 µm = 2 mils.

Figure 33. Photomicrograph. Pitting corrosion hollowed out the top layer of stainless steel 2304 exposed to $MgCl_2$ droplet.

The surface of stainless steel 2205 had small pits and shallow etched areas with NaCl exposure, as shown in figure 34. The corrosion damage to the steel was rather superficial, as shown in figure 35. The duplex stainless steel 2205 showed no sign of SCC or pitting (figure 36, figure 37, and figure 38).

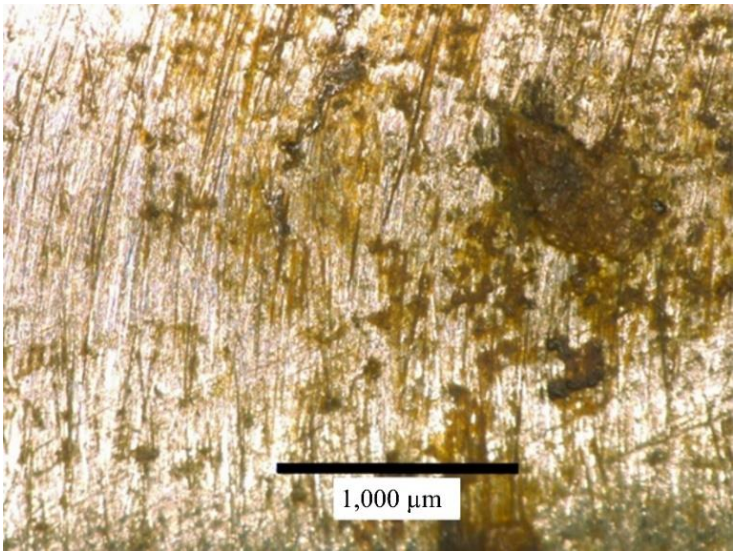

Source: FHWA.
1,000 µm = 39 mils.

Figure 34. Photomicrograph. Pitting corrosion on stainless steel 2205 exposed to NaCl droplet.

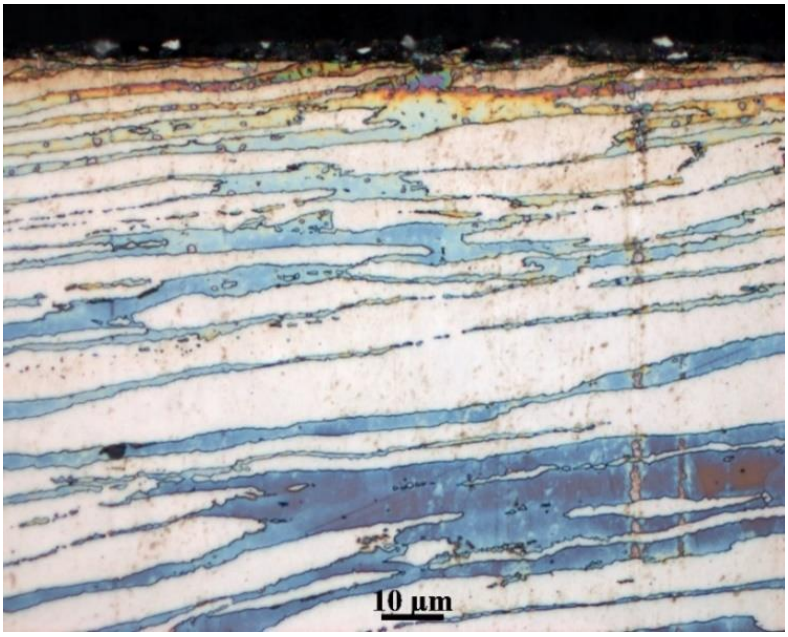

Source: FHWA.
10 µm = 0.4 mil.

Figure 35. Photomicrograph. Corrosion in the surface layer of stainless steel 2205 exposed to $MgCl_2$ droplet.

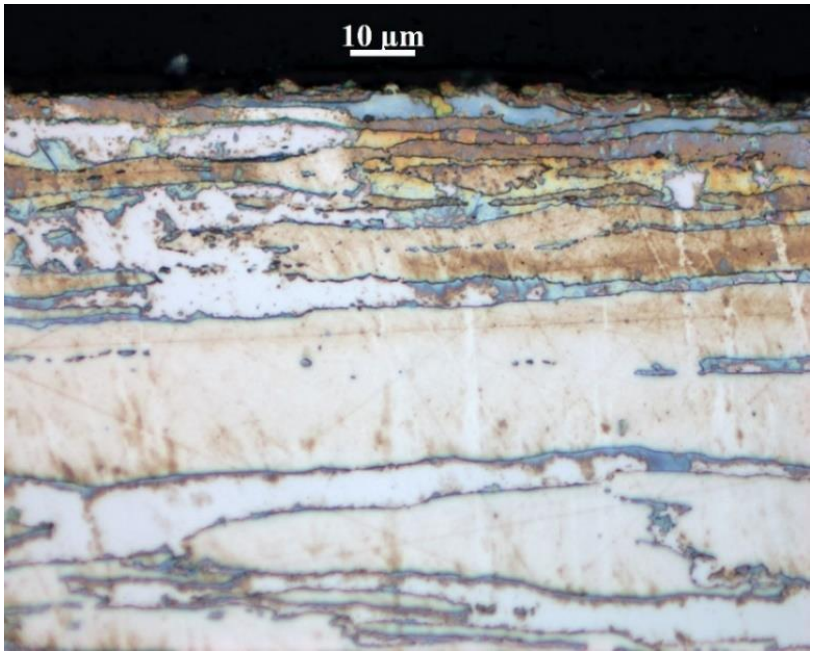

Source: FHWA.
10 µm = 0.4 mil.

Figure 36. Photomicrograph. No corrosion damage in stainless steel 2205 exposed to $CaCl_2$ droplet.

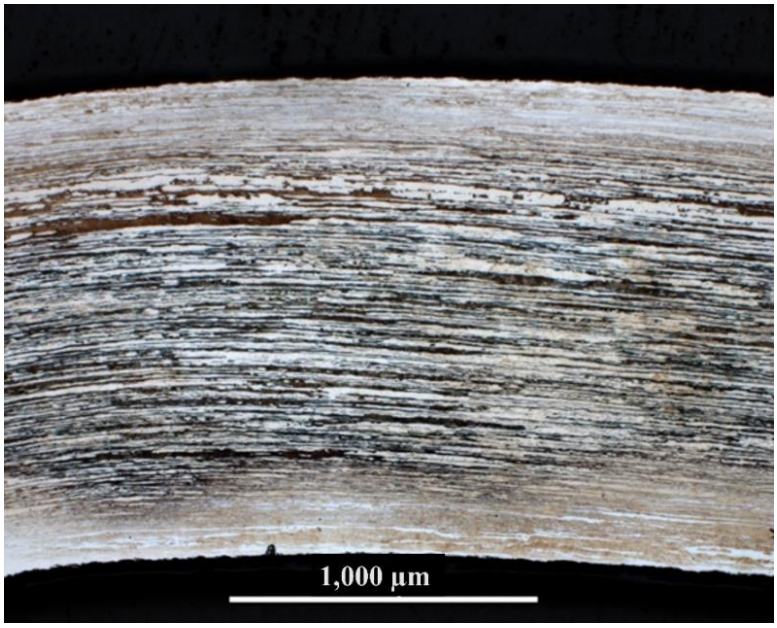

Source: FHWA.
1,000 µm = 39 mils.

Figure 37. Photomicrograph. No crack in stainless steel 2205 exposed to NaCl droplet.

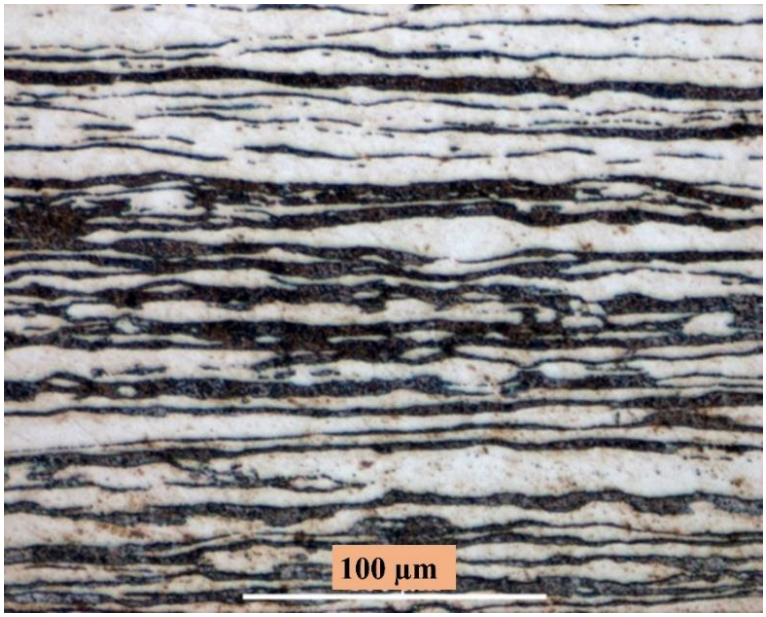

Source: FHWA.
100 µm = 4 mils.

Figure 38. Photomicrograph. High magnification showing no crack in stainless steel 2205 exposed to NaCl droplet.

Cracking Development Under High-pH Droplets

Localized corrosion or SCC developed on austenitic stainless steels after 9 w of exposure to high-pH chloride solutions $MgCl_2$ and $CaCl_2$. Small cracks were observed in 304L and 316LN.[1] Pits about 50 µm (2 mils) formed in XM-28.[1] Gorges longer than 1 mm (39 mils) were also present on the surface. After 16 w, the major cracks on 304L and 316LN widened and branched out. The pits on XM-28 grew much deeper, and etched valleys grew longer and deeper. After 1 yr of exposure, the cracks in 304L and 306LN severed the cross section of the U-bend, and the pits on XM-28 perforated the steel plates in multiple locations.

The high-pH NaCl solution did not cause SCC in any of the stainless steel grades, although superficial pitting corrosion was found on all the U-bends except XM-28. NaCl developed aggressive pitting corrosion on XM-28.

The duplex stainless steels were able to resist SCC, and no SCC was observed after 1 yr of exposure. After 16 w of exposure to $CaCl_2$, 0.5-mm (20-mil)-diameter pits developed on 2205. Surface etching and corroded valleys were also present on 2205 and 2304[1] at the same time. In general, the degree of localized corrosion damage caused by $MgCl_2$ and NaCl was less severe than that for $CaCl_2$.

Cracking Development Under Neutral-pH Droplets

Localized corrosion or SCC developed on austenitic stainless steels after 8 w of exposure to neutral-pH chloride solutions $MgCl_2$ and $CaCl_2$. Cracks initiated from pits on 304L and 316LN.[1] Pits, together with gorges, were present on XM-28.[1] After 12 w, the major cracks on 304L and 316LN had widened and branched out. After 25 w, the cracks had penetrated the depth and width of the U-bends, severing them in half.

NaCl droplets also caused pitting corrosion on 304L and316LN, although no SCC was observed. After 8 w of exposure to NaCl, 304L developed pits with a 100-µm (4-mil) diameter; 316LN had no visible pits. After 12 w of exposure, the pits on 304L grew numerous, and pits also appeared on 316LN.

Numerous pits were present on XM-28 after 8 w of exposure to NaCl, with diameters less than 40 µm (1.6 mils). After 12 w of exposure, the pits on XM-28 grew to 1-mm (39-mil) deep, and their shapes became irregular. After 25 w, the pits on XM-28 grew larger and deeper but did not perforate the steel plate. The neutral-pH NaCl solution did not cause SCC on XM-28.

The duplex stainless steels were able to resist SCC under neutral-pH chloride solutions. After 8 w of exposure to $MgCl_2$, a few pits developed on 2304,[1] and the diameters of the pits were less than 100 µm (3.9 mils). Some pits with diameters less than 50 µm (2 mils) also developed on 2205,[1] together with small etched areas of about 0.4 mm^2 (0.0006 in^2) or smaller. After 12 w, the number of small pits on 2304 grew, and etched areas of 1 mm^2 (0.0016 in^2) were also visible. At the same time, some 50-µm (2-mil)-diameter pits on 2205 grew deeper, and etched areas of about 1 mm^2 (0.0016 in^2) were visible. After 25 w, the pits and etched areas did not seem to change significantly.

The localized corrosion caused by $CaCl_2$ was similar to that of $MgCl_2$. After 8 w, a few pits were visible on 2304 and 2205 but were 50 µm (2 mils) in diameter or smaller. After 12 w, etched areas of 1 mm^2 (0.0016 in^2) were present on 2304, and a few shallow pits with 0.5-mm (20-mil) diameters were found on 2205. After 25 w of exposure, no significant changes were visible, although more black-colored corrosion product accumulated on the surface.

NaCl also caused pitting and surface etching on the duplex stainless steels. After 8 w, many small pits were visible on 2304 and 2205, and their diameter was less than 50 µm (2 mils). After 12 w, 2304 developed 1-mm^2 (0.0016-in^2) etched areas, and the number of pits grew. The 2205 also developed pits, and the pits and corrosion products formed dark-colored lines. Some corroded areas were about 0.75 mm (30 mils) in diameter. After 25 w of exposure, some pits grew slightly, and more corrosion products formed on the surface of the specimens. In general, the degree of localized corrosion damage caused by NaCl was as severe as that caused by $MgCl_2$ or $CaCl_2$.

PITTING POTENTIAL

Pitting is a form of localized corrosion that occurs on metals with protective films. Pitting manifests signs of attack with localized holes on the metal's surface. The holes can propagate in the metal rapidly, while other parts of the metal surface remain free from corrosion. The presence of chloride on the metal vigorously enhances pitting corrosion in some stainless steels.

An electrochemical method called cyclic potentiodynamic polarization provides simple and fast measurements to determine a metal's relative susceptibility to pitting corrosion. The test method is described in ASTM G61[(23)] and ASTM F746.[(24)] As the anodic potential moves in the more noble direction and passes the passive region, the anodic current increases rapidly, indicating localized pitting corrosion has initiated. This characteristic potential is defined as critical pitting potential and is broadly used to estimate the tendency of metal to develop localized corrosion. The more noble the critical pitting potential, the less likely pitting corrosion initiates on the metal.

The critical pitting potential was measured following ASTM G61 and ASTM F746. The test was carried out at 50 °C (122 °F), and the electrolyte was a 3.56-percent (by weight) NaCl solution. Figure 39 presents the results for stainless steels 304L, 316LN, and XM-28. Stainless steel 316LN has the most noble critical pitting potential among the three, while the least noble belongs to XM-28. The critical pitting potential for 304L is slightly more noble than that for XM-28. Figure 40 shows the critical pitting potentials for stainless steels 2205 and 2304. Within the tested potential range, the 2205 curve does not have a potential where the current increases rapidly, meaning pitting corrosion does not initiate. By comparison, stainless steel 2304 has reached its critical pitting potential, and pits initiated on the steel surface. Even so, 2304 has a more noble critical pitting potential that the three steels shown in figure 39.

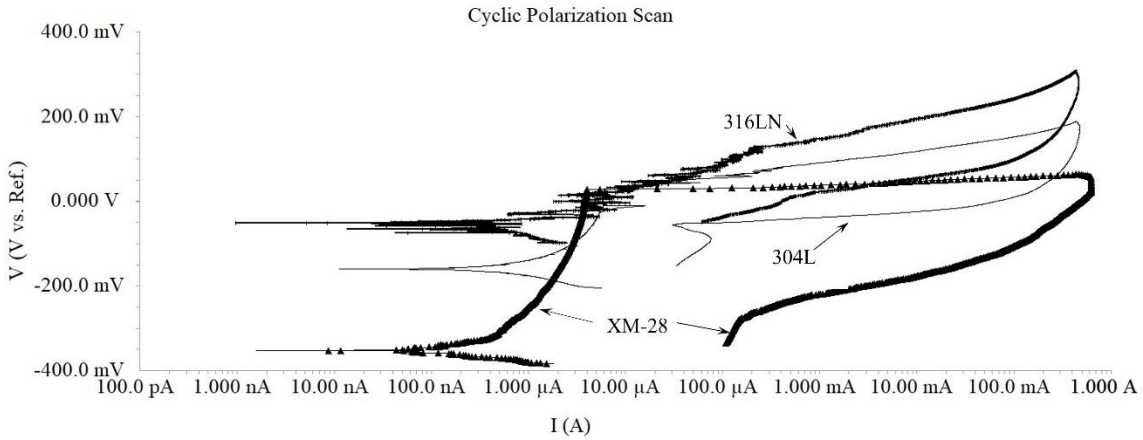

Source: FHWA.
Ref. = reference potential; *V* =voltage; *I* = current.

Figure 39. Graph. Critical pitting potential curves for 304L, 316LN, and XM-28 stainless steels in NaCl solution.

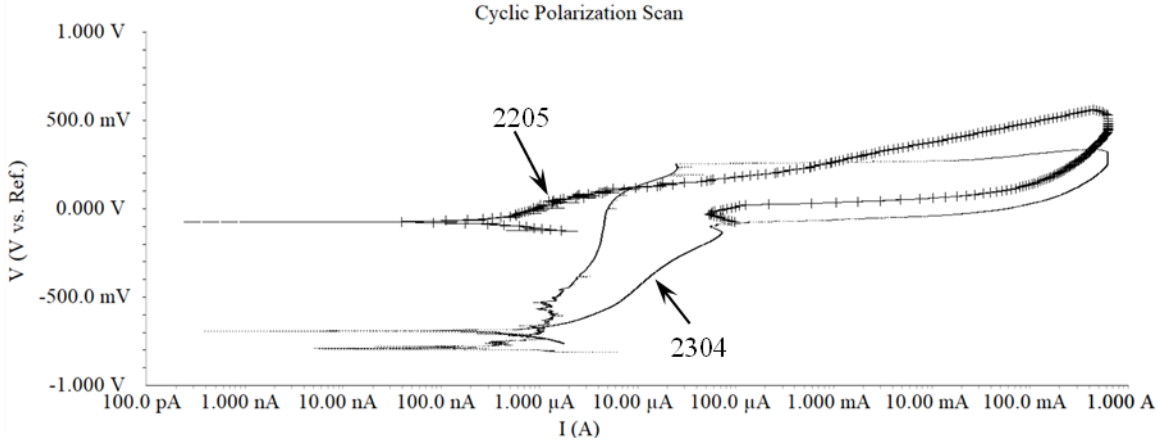

Source: FHWA.

Figure 40. Graph. Critical pitting potential curves for 2304 and 2205 stainless steels in NaCl solution.

The pitting resistance equivalent number (PREN) is a measure of the relative pitting corrosion resistance of stainless steel in a chloride-containing environment.[(25)] Stainless steel's pitting resistance is primarily determined by its chemical composition. The elements that have a significant impact are Cr, Mo, and N. The PREN is calculated as:

$$PREN=Cr+3.3Mo+16N$$

Higher PREN values indicate greater corrosion resistance. The PREN is listed in table 5, and the chemical composition data were provided in the mill report.

Table 5. PREN of the stainless steels.

Stainless Steel Grade		Alloying Chemical Composition (percent weight)				
ASTM	**UNS**	**Cr**	**Mo**	**Ni**	**N**	**PREN**
304L	S30403	18.2	0.3	8.0	0.08	21
316LN	S31653	17.7	2.1	10.2	0.12	26
XM-28	S24100	18.1	0.0	1.0	0.29	23
2304	S32304	22.8	0.3	3.6	0.17	26
2205	S32205	21.6	2.6	4.7	0.18	33

CHAPTER 4. SUMMARY AND CONCLUSION

SUMMARY OF FINDINGS

Austenitic Stainless Steel

The experiments showed that austenitic stainless steels 304L and 316LN[(1)] developed SCC when exposed to $MgCl_2$ and $CaCl_2$ at 50 °C (122 °F).

The cracking damage caused by $CaCl_2$ deposits was more extensive (aggressive) than that caused by $MgCl_2$ deposits. Multiple cracks developed under the $CaCl_2$ droplet, and each major crack then branched out extensively, penetrating deep into the bulk of the steel, with some cutting though the depth of the steel specimen.

The corrosion damage on 304L and 316LN caused by NaCl was limited to shallow pits and surface etching. SCC did not develop in these stainless steel samples exposed to NaCl. The chloride concentration in the NaCl droplet was half of the concentration in $MgCl_2$ and $CaCl_2$.

SCC did not develop in XM-28.[(1)] XM-28 is an austenitic stainless steel alloyed with high manganese and low Ni and is strengthened by extra N present in a solid solution. High N provides significantly higher tensile strength and yield strength without adversely affecting ductility. XM-28 has almost twice the yield strength of 304 stainless steel, which may have contributed to the resistance to SCC in the samples.

Localized corrosion perforated the samples exposed to NaCl. NaCl caused more aggressive pitting corrosion on the XM-28 than $MgCl_2$ and $CaCl_2$ did. The samples exposed to $MgCl_2$ developed deep pits. Pitting corrosion also appeared on $CaCl_2$-deposited samples, but the pits were much shallower. XM-28 seems to be prone to pitting corrosion, and pitting corrosion propagates faster at a relatively lower chloride concentration and higher relative humidity.

At 50 °C (122 °F), the relative humidity at the deliquescence point was 30 percent for $CaCl_2$, 35 percent for $MgCl_2$, and 75 percent for NaCl.

Based on the observation of corrosion damages to the stainless steel samples, $CaCl_2$ was the most aggressive solution to cause SCC compared with $MgCl_2$ and NaCl. $MgCl_2$ was relatively less aggressive, but still initiated SCC. The stainless steel samples exposed to NaCl did not develop SCC. NaCl did cause varying degrees of pitting corrosion on all austenitic stainless steels.

The pitting corrosion was most severe on XM-28. Shallow pits were found on 304L and 316LN. The researchers found no clear relationship between PREN and pitting among the austenitic stainless steels. The PREN followed the order 316LN > XM-28 > 304L, but the pitting corrosion damage from severe to mild was XM-28 > 304L > 316LN. The reason for the XM-28 being prone to pitting corrosion was not clear, but the researchers noticed that XM-28 contains much less Ni (1 percent) than 304L (8 percent) and 316LN (10 percent) do. Ni-based alloys are generally classified as corrosion-resistant alloys that resist low-temperature aqueous corrosion.

The experimental results demonstrated that SCC in austenitic stainless steel was associated with the stainless steel grade, the type of salt applied, and relative humidity; although the latter two factors were interconnected when the condition was kept at the deliquescence point of the salt. The concentration of the chloride ions in the surface solution was directly related to the aggressiveness of the salt droplets. At the deliquescence point, salt crystals absorb water molecules from the atmosphere to form a saturated solution.[12] However, the salt crystals remain dry if the relative humidity in the atmosphere is lower that the salt's deliquescence point. The most hygroscopic salt forms saturated solution at the lowest relative humidity. With increased humidity in the air, the salt crystals absorb more water molecules, the volume of the solution increases, and the concentration decreases.

The temperature and relative humidity data collected from the experiments shed light on the deliquescence point of the salts. At 50 °C (122 °F), $CaCl_2$ reaches equilibrium at 30-percent relative humidity, meaning the $CaCl_2$ droplet on the stainless steel absorbs the same amount of water molecules as it gives back to the atmosphere. Therefore, the volume of the droplet is constant, which leads to a constant concentration. The relative humidity was 35 percent at equilibrium for $MgCl_2$ and 75 percent for NaCl.

Research showed that at 50 °C (122 °F), the deliquescence points of the solutions are as follows: $CaCl_2$ is 13 percent relative humidity and 23.8 M chloride concentration; $MgCl_2$ is 28 percent relative humidity and 12.4 M chloride concentration; and NaCl is 75 percent relative humidity and 6.4 M chloride concentration. Clearly, $CaCl_2$ creates the highest concentration chloride solution and is, therefore, the most corrosive among the salts.

When temperature is constant, with increased humidity the chloride concentration decreases, and the corrosiveness of the salt droplets decrease as well. In contrast, when the humidity is lower than the dew point, water evaporates, the droplet becomes oversaturated, and salt crystals form. The experiment showed that for NaCl, when the humidity was lower than 75 percent, the droplet evaporated, leaving dry crystals on the stainless steel surface. Therefore, the chloride concentration at equilibrium is 6.4 M, which is too low to initiate SCC but is corrosive enough to cause pitting corrosion on the austenitic stainless steels.

Austenitic-Ferritic Stainless Steels

The duplex stainless steels 2205 and 2304[1] were resistant to SCC. However, the researchers observed localized corrosion on the steels. In addition to the small pits present on the steel surface, the team also found areas with shallow deterioration (as shown in figure 41 and figure 42 for 2304 and figure 43 and figure 44 for 2205), which Prosek, Iversen, and Taxen described as "etched zones."[13] They found that the etched zones were often elongated in the same direction as the cracks on the austenitic stainless steel. This direction is perpendicular to the plane of residual stress of the U-bend.

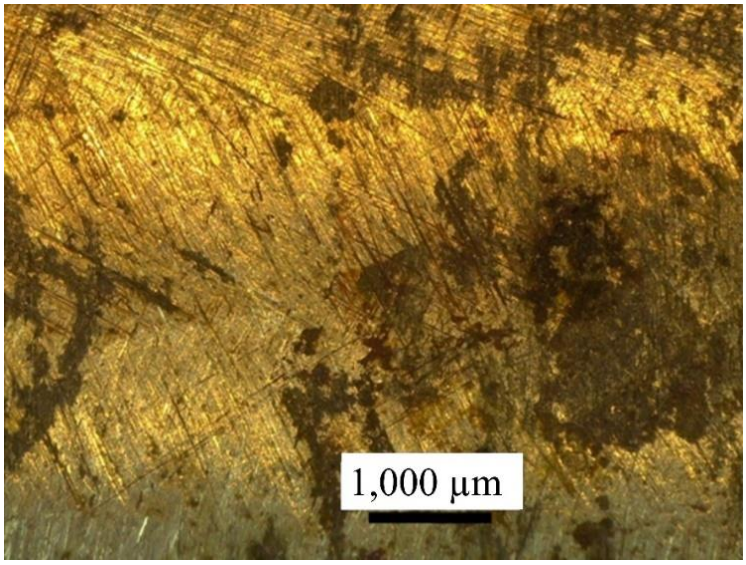

Source: FHWA.
1,000 µm = 39 mils.

Figure 41. Photomicrograph. Pitting corrosion on stainless steel 2304 exposed to $CaCl_2$ droplet.

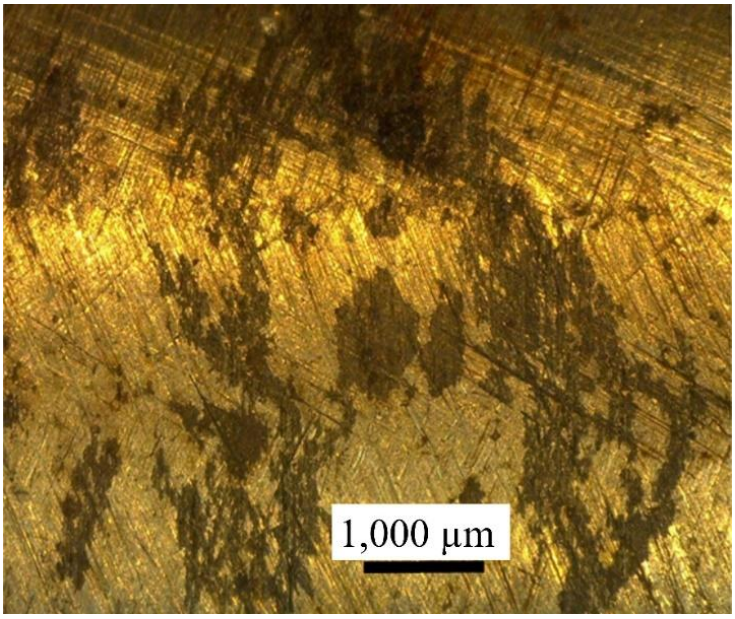

Source: FHWA.
1,000 µm = 39 mils.

Figure 42. Photomicrograph. Etched zones on stainless steel 2304 exposed to $CaCl_2$ droplet.

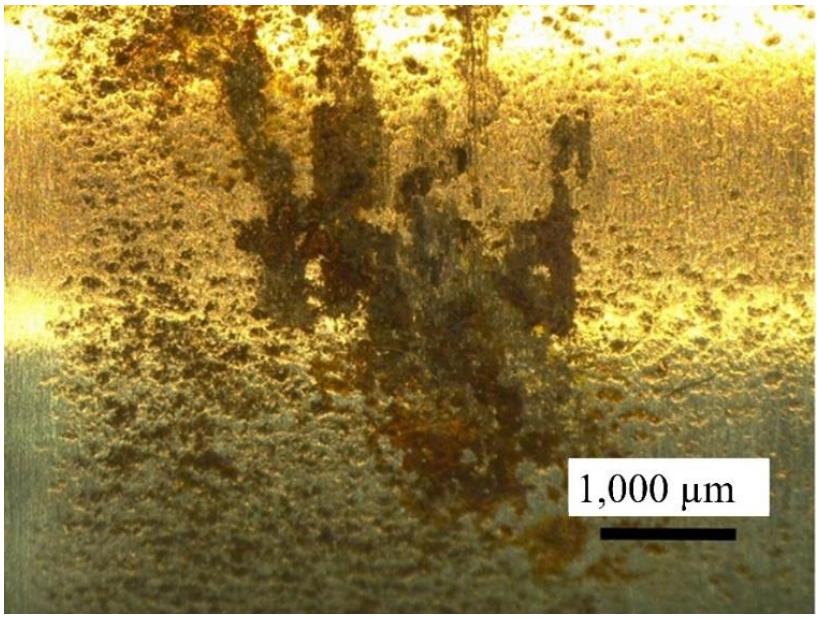

Source: FHWA.
1,000 µm = 39 mils.

Figure 43. Photomicrograph. Etched zone and pitting corrosion on stainless steel 2205 exposed to $MgCl_2$ droplet.

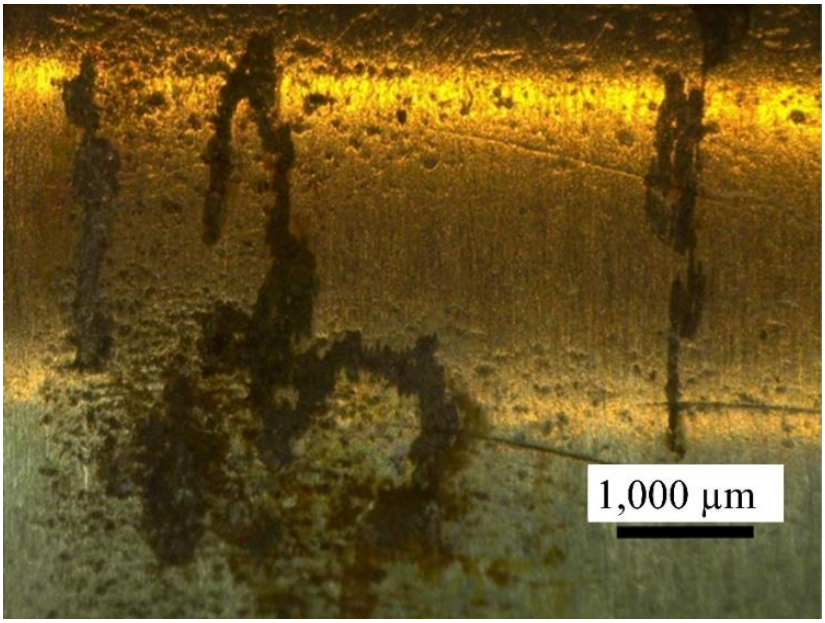

Source: FHWA.
1,000 µm = 39 mils.

Figure 44. Photomicrograph. Etched zones and pitting corrosion on stainless steel 2205 exposed to $MgCl_2$ droplet.

The localized corrosion on the U-bend specimens developed “ridges and valleys” along the longer dimension of the steel, which is parallel to the plane of the residual stress, as shown in figure 45 through figure 48. These ridges and valleys were found on both 2304 and 2205 stainless steels[1] exposed to more aggressive environments (i.e., $MgCl_2$ and $CaCl_2$). The researchers did not observe this form of corrosion on austenitic stainless steel specimens in this study.

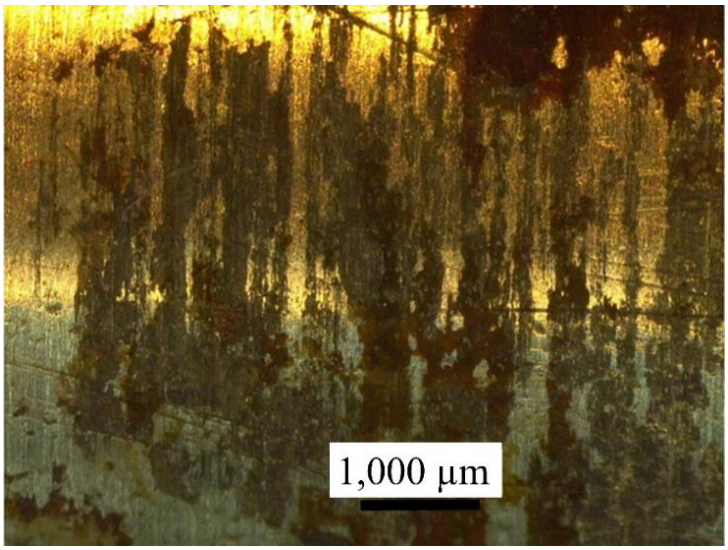

Source: FHWA.
1,000 µm = 39 mils.

Figure 45. Photomicrograph. Etched zones and small pits on stainless steel 2304 exposed to $CaCl_2$ droplet.

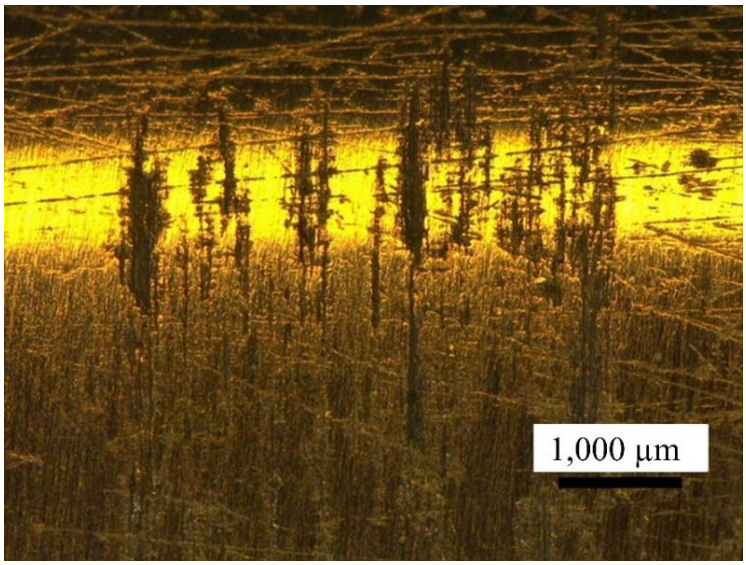

Source: FHWA.
1,000 µm = 39 mils.

Figure 46. Photomicrograph. Etched zones and pits on stainless steel 2304 exposed to $MgCl_2$ droplet.

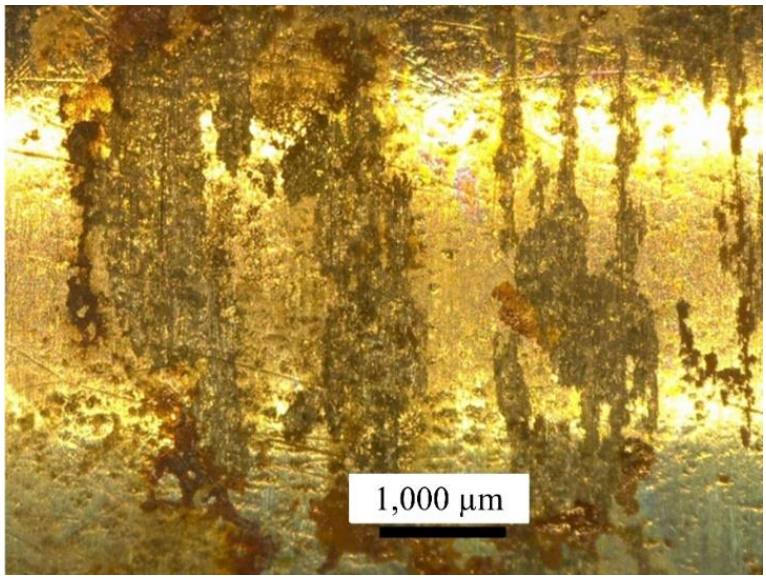

Source: FHWA.
1,000 µm = 39 mils.

Figure 47. Photomicrograph. Etched zones and pits on stainless steel 2205 exposed to $CaCl_2$ droplet.

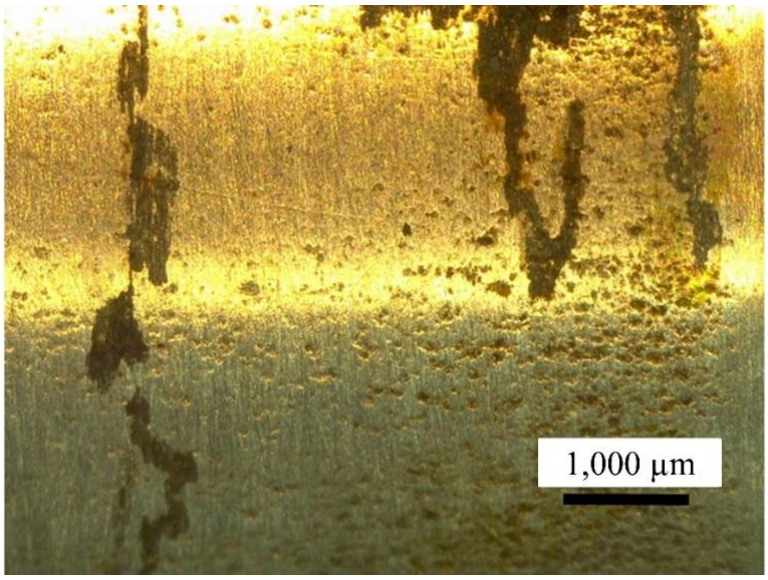

Source: FHWA.
1,000 µm = 39 mils.

Figure 48. Photomicrograph. Etched zones and pits on stainless steel 2205 exposed to $MgCl_2$ droplet.

Small areas of the surface layer were found to be selectively corroded in addition to the superficial etching and small pits. The 2304 stainless steel had pits 20 µm (0.8 mil) deep. Hollowed-out spots were also found in 2304, with a depth of about 50 µm (2 mils). The ferritic phase was selectively corroded (or selective dissolution), while the austenitic phase seemed

intact. The superficial corrosion (or dissolution) on 2205 was less pronounced than on 2304: only the surface suffered minor metal loss of less than 10 µm (0.4 mil). The superficial corrosion and the aggressiveness of the chloride droplets had no clear coordination. For example, NaCl caused as much corrosion as $CaCl_2$ on the 2205 steel surface.

Other researchers (Örnek, Zhong, and Engelberg, along with Prosek et al.) found SCC in duplex stainless steel exposed to chloride-containing droplets. [18,19] Örnek, Zhong, and Engelberg used $MgCl_2$:$FeCl_3$ (ferric chloride) droplets on 2205 stainless steel to study chloride-induced SCC.[18] The specimen was put under a direct tension rig to achieve 0.3-percent strain. The specimen was exposed to 50 °C (122 °F) and 30-percent relative humidity for 368 d. The $FeCl_3$:$MgCl_2$ droplet (0.68:1 mol ratio) contained 0.4 M chloride, calculated based on the data given in the paper. Multiple forms of corrosion were also present, such as selective dissolution, hydrogen embrittlement of the ferrite, pitting/crevice, and chloride-induced SCC of the austenite.

Cracks between tens of nanometers and tens of micrometers long were found in ferrite and austenite. Most cracks were arrested or diverted at the phase boundaries.[26] Örnek and Engelberg did not find SCC in 2205 when $MgCl_2$ was used in the droplet even at 80 °C (176 °F) and 27-percent relative humidity for 212 h.[26] However, Örnek et al. found SCC in 2205 after the steel was exposed to $MgCl_2$ at atmosphere 50±1 °C (122 ±2 °F) and 30±3-percent relative humidity for 512 and 615 d.[27] Örnek, Zhong, and Engelberg observed the effect of tensile loading on the development of discrete anodic and cathodic sites with the introduction of strain.[18] Örnek and Engelberg further state, "This observation supports the concept of an enhanced propensity of local electrochemical activity with increasing applied strain in duplex stainless steel."[28]

Prosek et al. studied SCC of austenitic and duplex stainless steels under $MgCl_2$ and $CaCl_2$ droplets.[19] They created the residual stress by circular welding on stainless steel plates. They found that at 70 °C (158 °F), SCC developed in duplex stainless steel grade 2205 but not in 2304.[1] They reasoned that selective corrosion of ferrite grains leads to stress relief in 2304, and since 2205 is more resistant to selective corrosion of the ferrite phase, 2205 does not contain stress relief. Prosek et al. concluded that the initiation of SCC and selective/pitting corrosion depended on the equilibrium chloride concentration in the droplet.

Findings from this study and others (i.e., Prosek's and Örnek's research) lead to the conclusion that the susceptibility of SCC in duplex stainless steel depends on the chloride concentration (therefore, the relative humidity of the air), temperature, and exposure time. (See references 18, 19, 26, and 27.)

CONCLUSION

The report conclusions are summarized as follows:

- Austenitic stainless steel grades 304L and 316LN[1] were susceptible to SCC when exposed to $MgCl_2$ and $CaCl_2$ at 50 °C (122 °F) and at a relative humidity approximating the deliquescent point. SCC in austenitic stainless steels 304L and 316LN was both intergranular and transgranular.

- XM-28[(1)] was not attacked by SCC; rather it developed severe pitting corrosion.

- Austenitic-ferritic duplex stainless steel grades 2304 and 2205[(1)] did not develop SCC. Selective dissolution of the ferrite phase was observed. Pitting corrosion and surface etching corrosion was superficial. The depth of corrosion damage was less than 20 µm (0.8 mil).

- PREN was a good indicator of SCC and pitting for both austenitic and duplex stainless steels, except for XM-28.

- High pH prolonged the time to initiation of SCC slightly, as the solution was carbonated in the air and pH decreased to slightly above neutral in a relatively short time. Corrosion reaction might have decreased the pH of the droplet even further.

- The corrosivity of the salts at their deliquescent point decreased in the order $CaCl_2$ > $MgCl_2$ > NaCl; the relative humidity increased in the same order.

- Pitting corrosion developed under the NaCl droplets, although NaCl did not cause SCC.

- SCC was closely associated with the metallurgical structure of the alloy, type of chloride salt and its concentration, temperature, and relative humidity.

REFERENCES

1. ASTM. 2024. *Standard Specification for Stainless Steel Bars and Shapes*. A276/A276M, West Conshohocken, PA: ASTM International.

2. Gewertz, M. W. 1958. "Causes and Repair of Deterioration to a California Bridge Due to Corrosion of Reinforcing Steel in a Marine Environment. I. Method of Repair." *Highway Research Board Bulletin* 182. https://onlinepubs.trb.org/Onlinepubs/hrbbulletin/182/182-001.pdf, last accessed March 7, 2024.

3. Spellman, D. L., and R. F. Stratfull. 1970. "Chlorides and Bridge Deck Deterioration." *Highway Research Record* 328: 38–49. https://onlinepubs.trb.org/Onlinepubs/hrr/1970/328/328-004.pdf, last accessed March 7, 2024.

4. McDonald, D. B., D. W. Pfeifer, and M. R. Sherman. 1998. *Corrosion Evaluation of Epoxy-Coated, Metallic-Clad and Solid Metallic Reinforcing Bars in Concrete*. Report No. FHWA-RD-98-153. Washington, DC: Federal Highway Administration.

5. Head, M., E. Ashby-Bey, K. Edmonds, S. Efe, S. Grose, and I. Mason. 2015. *Stainless Steel Prestressing Strands and Bars for Use in Prestressed Concrete Girders and Slabs.* Report No. MD-13-SP309B4G. Baltimore, MD: Maryland State Highway Administration. https://www.roads.maryland.gov/OPR_Research/MD-13_SP309B4G_Stainless-Steel-Prestressing-Strands_Report.pdf, last accessed March 7, 2024.

6. Kahl, S. 2011. *Stainless and Stainless-Clad Reinforcement for Highway Bridge Use*. Report No. RC-1560. Lansing, MI: Michigan Department of Transportation.

7. FHWA. 2009. "Simple Bridge Design Uses High-Performance Materials." *Innovator*, October/November 2009. Publication No. HIF-09-035. https://www.fhwa.dot.gov/innovation/innovator/issue15/issue15.pdf, last accessed August 19, 2022.

8. FHWA. 2012. "Vermont Sets Stainless Standard for Bridges." *Innovator*, May/June 2012. Publication No. HIF-12-002. https://www.fhwa.dot.gov/innovation/innovator/issue30/issue30.pdf, last accessed August 19, 2022.

9. Vermont Agency of Transportation. 2018. *2018 Standard Specifications for Construction*. Montpelier, VT: Vermont Agency of Transportation, pp. 5-77–5-81.

10. Rincon Troconis, B. C., S. R. Sharp, H. Celik Ozyildirim, C. R. Demarest, J. Wright, and J. R. Scully. 2020. *Corrosion-Resistant Stainless Steel Strands for Prestressed Bridge Piles in Marine Atmospheric Environments*. Report No. FHWA/VTRC 20-R2. Charlottesville, VA: VTRC. https://vtrc.virginia.gov/media/vtrc/vtrc-pdf/vtrc-pdf/20-R2.pdf, last accessed August 8, 2024.

11. Roberge, P. R. 2012. *Handbook of Corrosion Engineering*, 2nd ed. New York, NY: McGraw-Hill.

12. Adamson, A. W., and A. P. Cast. 1997. *Physical Chemistry of Surfaces*, 6th ed. New York, NY: John Wiley & Sons, p. 284.

13. Prosek, T., A. Iversen, and C. Taxen. 2008. "Low-Temperature Stress Corrosion Cracking of Stainless Steel in the Atmosphere in the Presence of Chloride Deposits." Presented at *CORROSION 2008, New Orleans, Louisiana, March 2008*, pp. 105–117.

14. Jones, D. A. 1996. *Principles and Prevention of Corrosion*, 2nd ed. New York, NY: Pearson, p. 258.

15. ASTM International. 2016. *Standard Practice for Making and Using U-Bend Stress-Corrosion Test Specimens*. G30-97. West Conshohocken, PA: ASTM International.

16. ACI Committee 318. 2022. *Building Code Requirements for Structural Concrete and Commentary (ACI 318-19).* Farmington Hills, MI: ACI.

17. ASTM International. 2019. *Standard Specification for Zinc-Coated (Galvanized) Steel Bars for Concrete Reinforcement*. A767/A767M. West Conshohocken, PA: ASTM International.

18. Örnek, C., X. Zhong, and D. L. Engelberg. 2016. "Low-Temperature Environmentally Assisted Cracking of Grade 2205 Duplex Stainless Steel beneath $MgCl_2$:$FeCl_3$ Salt Droplet." *Corrosion* 72, no. 3: 384–399.

19. Prosek, T., A. Le Gac, D. Thierry, S. Le Manchet, C. Lojewski, A. Fanica, E. Johansson, et al. 2014. "Low-Temperature Stress Corrosion Cracking of Austenitic and Duplex Stainless Steels Under Chloride Droplets." *Corrosion* 70, no. 10: 1052–1063.

20. Ge, Z., A. S. Wexler, and M. V. Johnston. 1998. "Deliquescence Behavior of Multicomponent Aerosols." *Journal of Physical Chemistry A*: 102, no. 1: 173–180.

21. ASTM International. 2020. *Standard Specification for Deformed and Plain Stainless Steel Bars for Concrete Reinforcement*. A955/A955M-20c. West Conshohocken, PA: ASTM International.

22. ISO. 2020. *Corrosion of Metals and Alloys—Evaluation of Stress Corrosion Cracking by the Drop Evaporation Test*. ISO 15324:2000. Geneva, Switzerland: ISO.

23. ASTM International. 2018. *Standard Test Method for Conducting Cyclic Potentiodynamic Polarization Measurements for Localized Corrosion Susceptibility of Iron-, Nickel-, or Cobalt-Based Alloys*. G61-86. West Conshohocken, PA: ASTM International.

24. ASTM International. 2014. *Standard Test Method for Pitting or Crevice Corrosion of Metallic Surgical Implant Materials*. F746-04. West Conshohocken, PA: ASTM International.

25. Francis, R. 2020. “Duplex Stainless Steels: The Versatile Alloys.” *Corrosion* 76, no. 5: 500–510.

26. Örnek, C., and Engelberg, D. L. 2015. “SKPFM Measured Volta Potential Correlated with Strain Localisation in Microstructure to Understand Corrosion Susceptibility of Cold-Rolled Grade 2205 Duplex Stainless Steel.” *Corrosion Science* 99: 164–171.

27. Örnek, C., F. Léonard, S. A. McDonald, A. Prajapati, P. J. Withers, and D. L. Engelberg. 2018. “Time-Dependent In Situ Measurement of Atmospheric Corrosion Rates of Duplex Stainless Steel Wires.” *npj Materials Degradation* 2, no. 10.

28. Örnek C, and Engelberg DL. 2016. “An Experimental Investigation into Strain and Stress Partitioning of Duplex Stainless Steel Using Digital Image Correlation, X-ray Diffraction and Scanning Kelvin Probe Force Microscopy.” *Journal of Strain Analysis for Engineering Design* 51, no. 3: 207–219. https://doi.org/10.1177/0309324716631669, last accessed July 8, 2024.

Recommended citation: Federal Highway Administration,
Exploratory Testing of Stress Corrosion Cracking in Stainless Steels at Low Temperature (Washington, DC: 2024) https://doi.org/10.21949/1521577

HRDI-10/09-24(WEB)E